

TOPICAL REVIEW

Electrostatics in soft matter

René Messina

Institut für Theoretische Physik II - Heinrich-Heine-Universität Düsseldorf,
Universitätsstr. 1, D-40225 Düsseldorf, Germany

E-mail: *messina@thphy.uni-duesseldorf.de*

Abstract. Recent progress in the understanding of the effect of electrostatics in soft matter is presented. A vast amount of materials contains ions ranging from the molecular scale (e.g., electrolyte) to the meso/macroscale one (e.g., charged colloidal particles or polyelectrolytes). Their (micro)structure and physicochemical properties are especially dictated by the famous and redoubtable long-ranged Coulomb interaction. In particular theoretical and simulational aspects, including the experimental motivations, will be discussed.

1. Introduction

Probably one of the most well known and understood ionic materials is sodium chloride (NaCl). In its *solid* form (i.e., NaCl cubic-like crystalline lattice), the experimentally measured heat of vaporization (7.92 eV) can be deduced (within about 10%) from a straightforward lattice sum of the form†

$$E_M = \frac{e^2}{4\pi\epsilon_0} \sum_{\text{lattice}} \frac{\alpha_j}{|\vec{r}_j|} \simeq -1.747 \frac{e^2}{4\pi\epsilon_0 a} \quad (1)$$

leading to the theoretical Madelung energy (here $E_M = -8.94\text{eV}$) [1, 2]. This striking good agreement demonstrates that electrostatics is indeed the relevant ingredient governing our ionic crystal [3]. In its *liquid* form, NaCl plays a fundamental role in soft matter, since it controls the degree of screening of the Coulomb interaction in all water based solutions. It is exactly this type of problem that this review will address: Electrostatics in soft matter.

Virtually all materials are more or less charged at the mesoscopic scale, depending on the degree of the polarizability of the embedding solvent (or matrix) and the solute particles (e. g., colloidal particles, polymers, membranes. etc.). The most well known example of polar solvent is evidently water which plays a crucial role in life, biological processes as well as industrial applications. When the solute particles are polar too, they can then dissociate into charged particles (also called *macroions*) and (*microscopic*) counterions. The counterion distribution near macroions turns out to be decisive for the surface properties of the latter.

The pioneering works of Gouy and Chapman [4, 5], realized almost one century ago, concern the counterion distribution near a planar charged interface. Applying the presently called Poisson-Boltzmann theory, they demonstrated that the counterion distribution profile decays algebraically as a function of the separation from the wall with a characteristic length that is inversely proportional to the surface charge density of the wall. Ten years later, Debye and Hückel [6] accomplished a fundamental advance towards the understanding of screening. This theory originally developed for electrolytes (i.e. a solution of microscopic cations and anions such as Na^+ and Cl^-) and based on the linearization of the Poisson-Boltzmann equation is now widely used in plasma and solid state physics.‡

Mean-field theories are appealing tools due to their intuitive and clear physical basis, and are robust theories as long as *electrostatic correlations* are not too important. In many practical situations (chromatin, polyelectrolyte multilayering, charged colloidal

† The resulting energy in equation (1) corresponds to the cohesive energy per NaCl molecule. An ion (either Na^+ or Cl^-) is placed at the origin and $\alpha_j = +, -$ depending on the type of ion sitting at the lattice position \vec{r}_j . $e = 1.602 \times 10^{-19}\text{C}$ stands for the usual elementary charge, $\epsilon_0 = 8.854 \times 10^{-12}\text{F/m}$ for the vacuum permittivity, and $a = 2.81\text{\AA}$ for the NaCl lattice parameter.

‡ Note that a similar potential of interaction (so-called Yukawa potential) arises at the subatomic scale to describe the cohesion of the nuclear matter. Nonetheless, in nuclear physics, the interpretation of this potential in terms of screening is not adequate.

suspension, etc.) electrostatic correlations are strong enough to make mean-field theories fail even on a qualitative level. Two striking and natural consequences of electrostatic correlations, that can not be explained by mean-field theories, are charge reversal (also called overcharging) and like charge attraction: (i) Overcharging concerns the situation where a macroion is locally covered by a cloud of counterions whose global charge overcompensates that of the macroion so that the net charge (or effective charge) changes sign; (ii) Like charge attraction is the counterintuitive effective attraction between two macroions carrying the same electric charge sign.

A colloidal suspension, the classical material of soft matter science, can crystallize via a strong enough mutual electrostatic repulsion. An understanding of the resulting phase behavior necessitates approaches where particle-particle correlations must obviously be taken into account. This constitutes another example where approaches going beyond the mean-field level are required.

The present work examines the problem of electrostatics in soft matter systems using simple theoretical models and computer simulations. The role of the little counterions is addressed in chapter 2. The relevance of excluded volume (i.e. the finite hard-core size of the constitutive ions) is discussed in chapter 3. The problem of image charges as occurring near curved dielectric interfaces is presented in chapter 4. The basic physics in more complex processes such as polyelectrolyte adsorption and multilayering is elucidated in chapter 5. Colloidal dispersions in strong confinement are presented in chapter 6. Finally, a conclusion and possible outlooks are provided in chapter 7.

2. Electrolyte at interfaces

2.1. Foundations of electrostatic mean field theories in soft matter

This part deals with the foundations of the electrostatic mean field theories in soft matter. It is written on a pedagogical level such that the non-specialist reader should be in a position to easily capture the underlying physics. Nonetheless, the expert will also certainly find some clarifying ideas in the forthcoming discussion.

2.1.1. Poisson-Boltzmann theory The model system we have here in mind is sketched in figure 1. We have to deal with a uniformly charged interface with a surface charge density σ , separating the semi-infinite substrate from a simple electrolyte [i.e. univalent cations (+) and anions (-)] and whose bulk density is ρ_0 . The system is globally electroneutral and the embedding solvent is merely characterized by its dielectric constant. In this context, the first theoretical determination of counterion distribution for an inhomogeneous fluid was realized by Gouy [4] and Chapman [5] independently almost one century ago. This mean-field approach corresponding to the so-called Poisson-Boltzmann theory is going to be now explained and discussed.

A central quantity in the statistical mechanics of fluids is the *potential of mean*

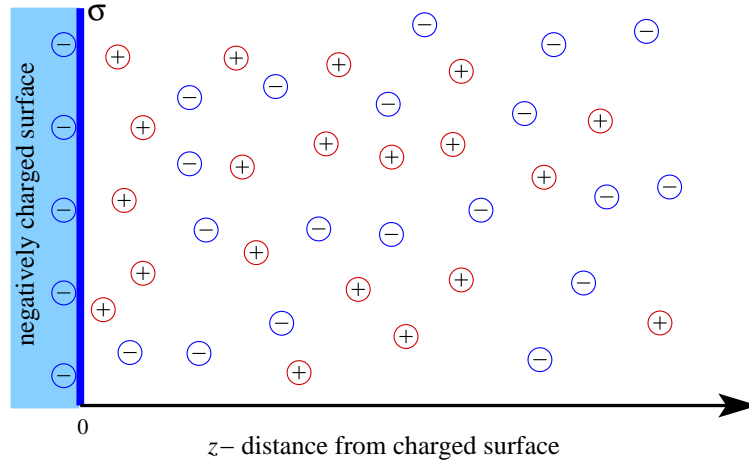


Figure 1. Model for a simple electrolyte near a (negatively) charged surface.

force (PMF). The latter corresponds to the potential stemming from the effective force between two objects. The term “effective” means here a thermodynamical averaging whose form is dependent on the ensemble (e.g., canonical, grand canonical) under consideration. For the sake of simplicity we will consider the thermodynamical (i.e., macroscopic) limit where all ensembles are equivalent.

A good starting point is provided by the exact Poisson equation relating the the mean electrostatic potential (MEP), $\psi(z)$, to the PMF $w_\alpha(z)$ as follows:

$$\Delta\psi(z) = -\frac{e\rho_0}{\epsilon_0\epsilon_{solv}} \{ \exp[-\beta w_+(z)] - \exp[-\beta w_-(z)] \}, \quad (2)$$

where ϵ_{solv} is the relative permittivity of the solvent (for water $\epsilon_{solv} \approx 80$), $\beta \equiv 1/(k_B T)$ the reduced inverse temperature with k_B being the Boltzmann constant and T the absolute temperature. The central approximation of the PB theory is to now set:

$$w_\pm(z) \stackrel{\text{(PB)}}{\simeq} \pm e\psi(z), \quad (3)$$

such that the exact Poisson equation (2) becomes in the framework of the PB theory:

$$\Delta\psi(z) = \frac{2e\rho_0}{\epsilon} \sinh[\beta e\psi(z)] \quad (\epsilon \equiv \epsilon_0\epsilon_{solv}) \quad (4)$$

which is the well known PB equation. The resulting MEP reads [7]:

$$\psi(z) = -\frac{2k_B T}{e} \ln \left[\frac{1 + \gamma \exp(-\kappa z)}{1 - \gamma \exp(-\kappa z)} \right], \quad (5)$$

where γ is given by the positive root of:

$$\gamma^2 + (2\kappa b)\gamma - 1 = 0 \quad \text{so that} \quad 0 \leq \gamma = -\kappa b + \sqrt{1 + (\kappa b)^2} < 1, \quad (6)$$

We have introduced here in equation (5) and equation (6) two important length scales, namely the screening length κ^{-1} :

$$\kappa^2 \equiv 8\pi\ell_B\rho_0 \quad (7)$$

and the Gouy-Chapman length b

$$b \equiv \frac{e}{2\pi\ell_B|\sigma|}, \quad (8)$$

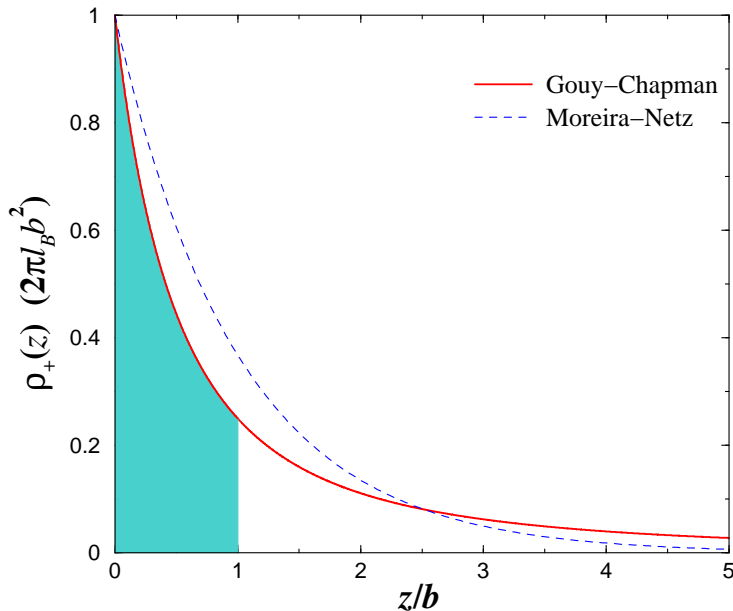


Figure 2. Reduced (Gouy-Chapman) counterion distribution $\rho_+(z)(2\pi\ell_B b^2) = \frac{1}{(1+z/b)^2}$ as given by equation (11). It is precisely at $z = b$, that the cumulated counterions (shaded region) half-compensate the charge of the surface. In other words, the counterion integrated charge at $z = b$ is exactly $-\sigma/2$. The strong Coulomb coupling limit (Moreira-Netz) $\rho_+(z)(2\pi\ell_B b^2) = \exp(-z/b)$ as given by equation (19) is also shown for direct comparison.

where ℓ_B is another third relevant length in charged soft matter known as the Bjerrum length[†] and reads:

$$\ell_B \equiv \frac{e^2}{4\pi\epsilon k_B T}. \quad (9)$$

The *salt-free* case can be actually easily obtained by considering $\kappa b \rightarrow 0$ in equation (5) and (6). Doing so we find:

$$\lim_{\kappa b \rightarrow 0} \psi(z) = \frac{2k_B T}{e} \ln[1 + z/b] + \frac{2k_B T}{e} \ln \frac{\kappa b}{2}. \quad (10)$$

The corresponding counterion distribution, $\rho_+(z) = \rho_0 \exp[-\beta e \psi(z)]$, is then merely given by:

$$\rho_+(z) = \frac{1}{2\pi\ell_B} \frac{1}{(z+b)^2}. \quad (\text{salt-free}) \quad (11)$$

It is this formula (11) that is referred to as the Gouy-Chapman counterion distribution. The corresponding plot can be found in figure 2.

To better understand the physical meaning involved in the approximation (3), we

[†] The physical interpretation of the Bjerrum length is straightforward: It is the distance between two elementary charges e that leads to an electrostatic interaction equating $k_B T$.

shall make use of the exact so-called Yvon-Born-Green (YBG) hierarchy [8] that reads:

$$-\vec{\nabla}_1 w_\alpha(z_1) = -\frac{q_\alpha |\sigma|}{2\epsilon} \vec{e}_z - \sum_{\beta=1}^2 \int \vec{\nabla}_1 \left[\frac{q_\alpha q_\beta}{4\pi\epsilon r_{12}} \right] g_{\alpha\beta}(r_{12}, z_1, z_2) \rho_\beta(z_2) d^3r_2 \quad (12)$$

Equation (12) can be seen as a “Newtonian” version of the statistical Poisson equation (2). The left hand-side of equation (12) represents the effective force felt by the test ion 1 of species $\alpha = \pm$ at prescribed location $\vec{r}_1 = (x_1, y_1, z_1)$. The right hand side of equation (12) is made up of two contributions: (i) The first term is merely the Coulomb interaction between the charged interface and the test ion 1. (ii) The second term involves the interaction between the test ion 1 and the remaining solute ions, with $g_{\alpha\beta}(\vec{r}_1, \vec{r}_2)$ being the pair distribution function and $\rho_\beta(z_2)$ the local ion density. If the former is approximated by $g_{\alpha\beta}(\vec{r}_1, \vec{r}_2) \approx 1$ then equation (12) becomes:

$$-\vec{\nabla}_1 w_\alpha(z_1) = -\vec{\nabla}_1 \underbrace{\left[q_\alpha \left\{ \frac{|\sigma|}{2\epsilon} z_1 + \sum_{\beta=1}^2 \int \frac{q_\beta}{4\pi\epsilon r_{12}} \rho_\beta(z_2) d^3r_2 \right\} \right]}_{=q_\alpha\psi(z_1)}, \quad (13)$$

so that the potential of mean force reduces to the MEP times the charge, which is precisely the PB approximation. In other words, the PB theory neglects the (lateral) *ion-ion correlations* in that sense that $g_{\alpha\beta}(\vec{r}_1, \vec{r}_2) = 1$.[†] It is for this reason that the PB theory is a mean-field one. Recalling that

$$g_{\alpha\beta}(r_{12}, z_1, z_2) \equiv \frac{\rho_{\alpha\beta}^{(2)}(r_{12}, z_1, z_2)}{\rho_\alpha(z_1)\rho_\beta(z_2)}, \quad (14)$$

where $\rho_{\alpha\beta}^{(2)}(r_{12}, z_1, z_2)$ is the two-particle density function, one can equally well provide a geometrical interpretation: The probability of finding two ions anywhere in the solution is *independent* of their relative separation in the PB framework.[‡]

2.1.2. Debye Hückel theory In general the strongly non-linear PB equation (4) can not be solved analytically, and its linearized version is therefore employed instead. This latter approach was historically first developed by Debye and Hückel [6]. When the MEP is everywhere small (i.e., $|e\psi| < 1$), the PB equation reduces to

$$\Delta\psi = \kappa^2\psi \quad (15)$$

and the corresponding solution reads:

$$\psi(z) = \psi_S e^{-\kappa z} = -\frac{4\gamma k_B T}{e} e^{-\kappa z}, \quad (16)$$

[†] Note that the existence of lateral ion-ion correlations [i.e., $g_{\alpha\beta}(\vec{r}_1, \vec{r}_2) - 1 \neq 0$] have two physical origins: (i) Electrostatics and (ii) steric effects due to excluded volume. The latter are implicitly ignored in the PB framework.

[‡] Clearly, the bare Coulomb pair force between all constitutive ions are properly taken into account in the PB theory, see equation (13). It is the assumption of a structureless lateral arrangement of the ions that creates the crucial inconsistency in the PB framework.

where ψ_S denotes the surface potential. This result can be obtained either by directly solving the DH equation (15) or substituting the small ψ_S value in the full PB solution equations (5) and (6).

In order to more deeply understand the physical meaning of the linear approximation, we shall rewrite the DH equation (15) in an equivalent integral equation form. In this context, it is instructive to use an approximative closure for the (exact) Ornstein-Zernike equation, as done by McQuarrie for a bulk electrolyte [9], which leads to the DH description:

$$h_{0\alpha}(z_1) = \underbrace{c_{0\alpha}(z_1)}_{\substack{\text{(DH)} \\ \approx -\alpha z_1/b}} + \sum_{\beta=1}^2 \rho_\beta \int h_{0\beta}(z_2) \underbrace{c_{\beta\alpha}(r_{12}, z_1, z_2)}_{\substack{\text{(DH)} \\ \approx -\alpha\beta\ell_B/r_{12}}} d^3r_2 \quad (17)$$

$$= \underbrace{c_{0\alpha}(z_1)}_{\substack{\text{(DH)} \\ \approx -\alpha z_1/b}} + \sum_{\beta=1}^2 \rho_\beta \int \underbrace{c_{0\beta}(z_2)}_{\substack{\text{(DH)} \\ \approx -\beta z_2/b}} h_{\beta\alpha}(r_{12}, z_1, z_2) d^3r_2, \quad (18)$$

where, the subscript “0” in equations (17) and (18) stands for the charged interface (that can be envisioned as a special particle species at infinite dilution). Thereby, this notation preserves nicely the analogy with the bulk case. The DH theory is readily obtained upon assuming that the direct correlation function is equal to the (sign reversed) reduced pair potential [i.e., $c(r) = -\beta V(r)$], which becomes exact when $\rho_0\ell_B^3 \rightarrow 0$ and $b/\ell_B \rightarrow \infty$. In practice it is the first line (17) that is used in fluid theory to solve self-consistently the total correlation function $h_{ij} \equiv g_{ij} - 1$ or the PMF via $h_{ij} \stackrel{\text{(DH)}}{\approx} -\beta w_{ij}$.

For the sake of our discussion, however, it is the second line (18) that turns out to be instructive. Indeed we see now that in the DH theory, the term $g_{\beta\alpha}(\vec{r}_1, \vec{r}_2)$ is not trivially unity, since $h_{\beta\alpha}(\vec{r}_1, \vec{r}_2)$ does not vanish in equation (18), in contrast to what happens in the PB situation. Hence ion-ion correlations are *not* neglected.† This might seem at first sight counter-intuitive since the DH theory is based on the linearization of PB equation which ignores lateral correlations. This being said, in the weak Coulomb regime where the DH theory is supposed to be valid, the deviations from the uncorrelated limit are then small.

2.2. Strong Coulomb coupling

2.2.1. Strong Coulomb coupling theories

This last decade [10, 11], a remarkable theoretical achievement has been accomplished in the other extreme limit of strong Coulomb coupling. More specifically, the counterion distribution near a charged planar wall has been predicted analytically and independently by Shklovskii [10] and Moreira and Netz [11] in the strong Coulomb coupling regime (i.e., the Gouy-Chapman problem at low temperature). A common and universal feature of these two works is that the

† Note that MacQuarrie used the very same method [equation (18)] to determine analytically (via Fourier transformation) the DH potential in spherical geometry [9]. However, in the past, he was not aware of the relevance of lateral ion-ion correlations, and therefore did not point out this issue.

counterion distribution decays exponentially like $\exp(-z/b)$. These two approaches are going to be now briefly presented.

- Using a field theoretic formulation applied to charged fluids [12, 13], Moreira and Netz [11] showed that at high Coulomb coupling (i.e.: for $\Xi \equiv \frac{\ell_B}{b} \gg 1$) the counterion distribution obeys the following *exact* and elegant limiting law:

$$\frac{\rho(z)}{2\pi\ell_B\sigma_s^2} = \exp(-z/b) \quad (19)$$

with $\sigma_s = |\sigma|/e$ (having the dimension of the inverse of a surface) standing for the number of elementary charges per unit area. A plot of equation (19) can be found in figure 2, where a convenient visual comparison with the high temperature limit [equation (11)] is offered.

- Using a fully different and more intuitive approach, Shklovskii [14] has applied Wigner crystal (WC) concepts [15, 16] to the problem of soft charged matter at effective low temperature. Using some heuristic but physically sound arguments, essentially based on the simple fact that a “desorbed” counterion from the (triangular) WC counterion layer is correlated to the hole left behind over the Gouy-Chapman length b , Shklovskii [14] obtains (up to the here important prefactor) the same result [equation (19)] as Netz. Interestingly, if one combines (i) the WC approach that provides the correct exponential decay $\exp(-z/b)$ and (ii) the contact theorem which imposes the prefactor, $2\pi\ell_B\sigma_s^2$ [17],[‡] then one recovers the exact answer (19).

2.2.2. Overcharging and Thomson problem As long as the Coulomb coupling between ions is “fairly” moderate (which is the case for monovalent ions in aqueous solution), the PB theory [4, 5, 18, 19] and even the DH one [20] describe astonishingly well the ion distribution (and hence the thermodynamical system properties) when compared to computer simulations [21, 22, 23, 24, 25, 26], theories going beyond the mean-field PB level [27], and even experiments [28]. Nonetheless, as soon as ion-ion correlations get relevant, mean field theories such as the PB one [29] or its linearized version (as related above in 2.1) can not explain the experimentally observed relevant effect of overcharging [30, 31].

Naively, one would think that the stable configuration corresponds to an exact neutralization of the macroion by the counterions. This intuition is only correct for the case where the counterions are uniformly smeared out over the surface of the colloid. Indeed basic electrostatics show that, for a central charge $Z_m e < 0$ (representing the macroion) and the shell of the counterions of radius a and (total) charge $Z_c^{(shell)} e > 0$, the electrostatic potential energy is given by [32]

$$E = \frac{Z_m Z_c^{(shell)} e^2}{a} + \frac{Z_c^{(shell)2} e^2}{2a}, \quad (\text{CGS}) \quad (20)$$

[‡] Note that $2\pi\ell_B\sigma_s^2 = \frac{1}{2\pi\ell_B b^2}$, so that the PB theory predicts the exact contact value as well [compare with equation (11)], see figure 2. This is not true, however, for the DH version.

where the first term describes the interaction between the central ion and the charged shell and the second one is the electrostatic energy stored in the shell (i.e., the work done upon bringing the counterions from infinity to their current location $r = a$ of the shell). Thereby, the criterion of stability

$$\frac{\partial E}{\partial Z_c^{(shell)}} = 0 \text{ and } \frac{\partial^2 E}{\partial Z_c^{(shell)2}} = e^2/a > 0 \quad \Rightarrow Z_c^{(shell)} = -Z_m \quad (21)$$

shows that the stable configuration corresponds to an exact neutralization. In reality, the counterions are *discrete* and not smeared out, and when electrostatically bound to the macroion's surface, they will maximize their separation such as to minimize the counterion-counterion repulsion. This problem turns out to be exactly the one that was addressed one century ago by Thomson [33] (also called the Thomson sphere or Thomson problem) who studied the ground state energy and structure of N (classical) electrons confined on a sphere (model of a classical atom). The Thomson problem has only exact solutions for small N and some magic numbers (e.g., $N = 72$ corresponding to the fullerene structure) [34]. Nonetheless, based on Wigner crystal ideas [15, 10, 35], an analytical model was developed which quantitatively accounts for the energy gain upon adsorbing overcharging counterions † [36, 32]. More precisely, the following relation for the energy variation ΔE_n (relative to the globally neutral state characterized by $n = 0$ overcharging counterion and $N = Z_m/Z_c$ counterions, see figure 3 for a typical counterion arrangement) as a function of the number n of (excess) overcharging Z_c -valent counterions [32] was derived:

$$\Delta E_n = -\frac{\alpha Z_c^2}{\sqrt{4\pi a^2}} [(N + n)^{3/2} - N^{3/2}] + \frac{Z_c^2 n^2}{2a}, \quad (\text{CGS}) \quad (22)$$

where α (≈ 2) is a numerical geometrical prefactor that was determined by simulations (deduced from the value of ΔE_1). ‡ The first and attractive term in equation (22) stems basically from the interaction between a counterion and its oppositely charged Wigner-Seitz cell. Energy profiles of equation (22) are sketched in figure 3, where one can see that these analytical predictions are pretty robust. This simple approach to the understanding of the overcharging via the Thomson problem, Wigner crystal concept and computer simulations has triggered a new interest in the community [37, 38, 39, 40] for the Thomson problem applied to soft matter.

We now consider the problem of a pair of macroions. In [36], it was shown that two equally charged spheres are likely to be overcharged and undercharged in the strong Coulomb coupling regime leading to a metastable *ionized state* that yields a strong long-ranged attraction due to a *monopolar* contribution. All the mechanisms,

† To achieve overcharging in nature one should normally add salt to the system to ensure global electroneutrality. For the sake of simplicity, however, we will consider non-neutral systems because they can, on a very simple basis explain, why colloids prefer to be overcharged.

‡ Note that in the case of vanishing curvature (i.e., $a/d_c \rightarrow \infty$ where d_c is the mean distance between counterions) our expression becomes exact since the planar WC limit is recovered for which $\alpha = 1.960516\dots$ [15].

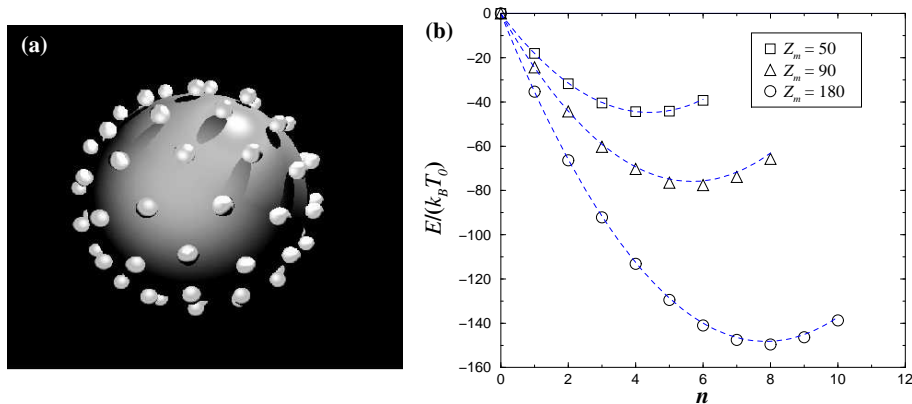


Figure 3. (a) Snapshot of the ground state structure with $Z_m = 180$ corresponding to $N = 90$ counterions. Note the local triangular arrangement on the “Thomson sphere”. (b) Electrostatic *ground state* energy (in units of $k_B T_0$ with T_0 being the room temperature) as a function of the number of *overcharging* counterions n for three different bare charges Z_m . The neutral case was chosen as the potential energy origin, and the curves were produced using the theory of equation (22), compare text. Data taken from [32].

so far reported in the literature, can only explain *short-ranged* like-charge attraction [41, 42, 43, 12, 44, 45, 46, 47, 14, 48, 49, 50, 51].

To further rationalize this phenomenon and the stability of ionized states [52, 32], two charged spheres of same radius a , carrying the same electric sign of charge but characterized by a charge ratio ρ_Z such that $0 < \rho_Z \equiv Z_B/Z_A \leq 1$, were considered. Starting from a macroion pair where each macroion is neutralized by its counterions, the process where a counterion is transferred from macroion B (low bare charge) to macroion A (high bare charge) was investigated [52, 32]. Having demonstrated that the ability of a macroion to get overcharged increases with growing (bare) surface charge density σ (or the bare charge at fixed radius), it is clear that this counterion-transfer process will be energetically favorable below a certain value of ρ_Z . This theoretical prediction shows that the criterion for stable ionized states (latter also called by other authors [39, 53] “auto-ionization”) is governed by the value of

$$\sqrt{N_A} - \sqrt{N_B} \gtrsim 1 \quad (23)$$

(with $N_{A/B} = Z_{A/B}/Z_c$ being the number of counterions of macroion A/B) which reflects the correlation-hole energy difference between the two macroions (at identical radii). In particular, it was demonstrated that the higher the charge-asymmetry (i.e., ρ_Z) the more stable the ionized state and concomitantly the higher the degree of ionization [52, 32]. The main findings related to this work [36, 52, 32], can be summarized as follows:

- The ground state of a charged sphere is always overcharged due to counterion correlations.
- At finite temperature and in the strong Coulomb regime (accessible with multivalent *aqueous* ions), colloids having different bare surface charge density auto-ionize due

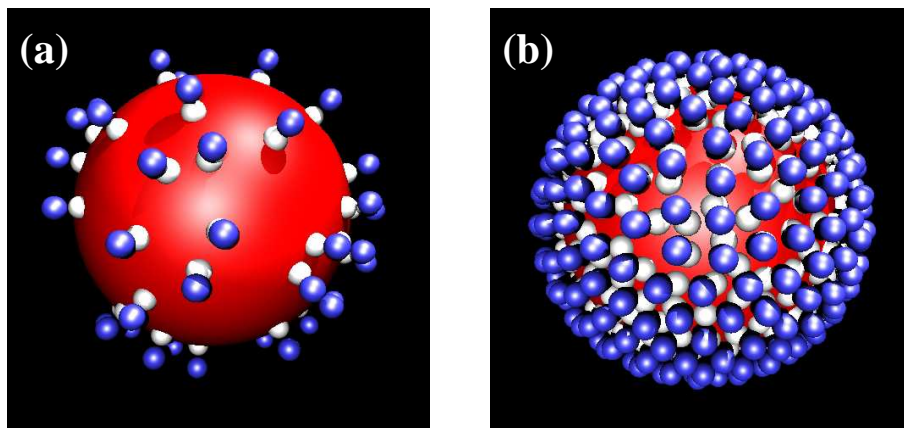


Figure 4. Computer simulation snapshots of counterion ground state configurations. The discrete colloidal surface charges are in white. The counterions are in blue. (a) “Low” and (b) “high” surface charge densities are shown. Data taken from [55].

to counterion correlations.

2.3. Discretely charged surfaces

The structural (i.e., bare) charge of spherical macroions is usually modeled by a *central* charge, which, by virtue of the Gauss’ law, is equivalent to a *uniformly* charged macroion surface as far as the electrostatic field (or potential) *outside* the sphere is concerned. However, in nature the charges on the colloidal surface are *discrete* (exactly as the counterions are) and localized, see figure 4. Thus, a natural question that rises is: *Why* and *how* does the counterion distribution depend on the way the structural charge of the macroion is represented (i.e., uniformly charged or discrete charges on its surface)? It is precisely this problem that was addressed in [54, 55].

Why is the counterion distribution sensitive to the choice of the representation of the macroion charge (discrete vs. uniform)? This question can be best answered by looking at and comparing the (intrinsic) electrostatic potentials generated by discretely and uniformly charged macroions (without counterions) [54]. It was demonstrated in Ref. [54] that the electrostatic potential at a reduced distance r/a from the sphere (where a stands for the distance of closest approach between an external unit test-charge and the macroion surface) may be significantly different according to the nature of the macroion charge. In particular we show that the higher the bare surface charge (i.e., the closer we get to a uniform charge distribution) the shorter the correlation length (typically $r_c \sim \sqrt{1/\sigma_s}$) between the discrete surface charges, as intuitively expected. More specifically, the contact potential is sensitive to the localization of the discrete charges, leading to a pronounced depth in their vicinity. All those features, solely based on the spatial behavior of the electrostatic potential stemming from the bare macroion, indicate that the counterion distribution should be much more complicated for a discrete macroion surface charge distribution than for the uniform case.

We now come to the other important question: *How* is the counterion distribution

modified when introducing the more realistic discrete macroion's surface charge distribution? This point is thoroughly addressed in [55], where two regimes are considered: Ground state ($T = 0$) and finite temperatures. The corresponding relevant findings [54, 55] can be summed up as follows:

- At zero temperature, the counterion (surface) structure possesses greater order the higher the reduced surface charge density σ_s and/or counterion valence Z_c are.
- When overcharging comes into play several scenarios occur: (i) At large σ_s , the overcharging is nearly the same as that obtained at a uniformly charged macroion's surface. (ii) At low σ_s and for *monovalent* counterions, overcharging is always weaker for discrete macroion charge distribution, due to the ion-pairing frustration for the excess counterions. (iii) At low σ_s and for *highly multivalent* counterions, overcharging can even be stronger in the discrete case due to ion-pairing.
- At finite temperature (in aqueous solutions), the volume counterion distribution is only affected for low σ_s and multivalent counterions.

The effect of surface charge discretization was later examined for different geometries by several groups [56, 57, 58, 59, 60, 61, 62].

3. The crucial role of excluded volume

3.1. Monovalent ions near a charged sphere

So far, we have had a pretty good understanding of the physics involved in the counterion distribution for *salt-free* systems where excluded volume effects are irrelevant. The situation becomes much more complicated at finite salt-concentrations in aqueous solutions (i.e., water at room temperature in the presence of added salt), where the Coulomb coupling is (rather) weak especially for monovalent ions. Thereby, a direct application of Wigner crystal ideas is not straightforward enough to account for the unexpected overcharging at *weak* Coulomb coupling that was reported theoretically [63, 64, 65, 66]), but unexplained, for *monovalent* salt-ions of large size.

Molecular dynamics computer simulations as well as integral-equation theory [67] were employed to identify the mechanisms that govern counterions ordering and overcharging in this weak Coulomb coupling regime. Those mechanisms are as follows:

- Increasing the electrolyte particle *size* (at given salt concentration) decreases the available volume of the fluid (or equivalently its entropy) which *favors ion-ion correlations*.
- The interface provided by the macroion causes an increase of the ion density close to it, and concomitantly enhances the *lateral ordering* (similar to the prefreezing phenomenon in *neutral* inhomogeneous fluids).
- Surface lateral ordering and (weak) Coulomb coupling lead to overcharging.

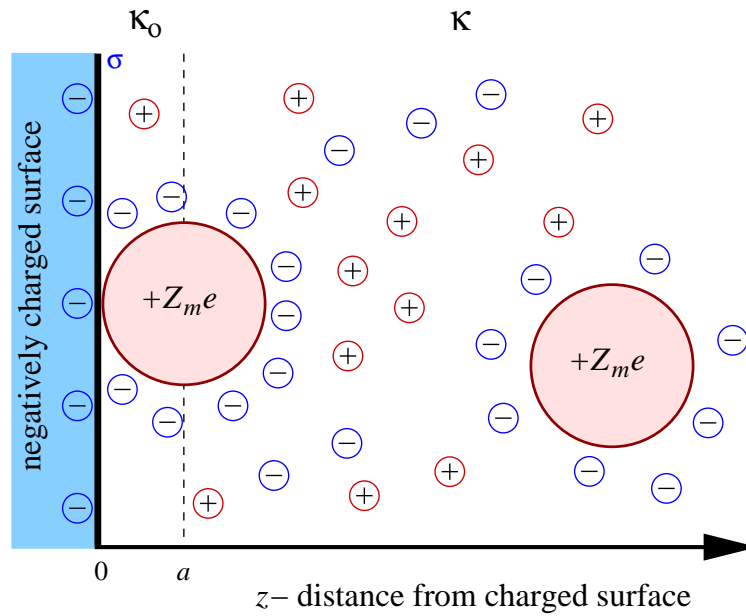


Figure 5. Schematic view of the electrostatic model for macroions near an oppositely charged interface. The macroions are characterized by a distance of closest approach $z = a$ to the charged surface, leading to two screening strengths κ_0 and κ for $0 < z < a$ and $z > a$, respectively.

3.2. Macroion adsorption at planar substrates

Excluded volume effects coupled to electrostatic interactions can also lead to counter-intuitive phenomena in the process of macroion adsorption. A description of the model setup is sketched in figure 5. For instance, Jimenez-Ángeles and Lozada-Cassou showed, using integral equation theory, that for moderately (attractive) charged substrates, a film of *coions* first builds up. The electrostatic consequence is that at the direct vicinity of the surface of the substrate its charge gets amplified (i.e., *surface charge amplification*). The driving force of this effect is due to the macroion-ion attractive correlations. † This effect was overlooked in the past, because the authors neglected either the finite size of the macroion [68] or the spatial distribution of the little salt-ions [69].

Recently, this problem was revisited by using a very simple analytical model based on the Debye-Hückel approximation *but* taking into account the finite size of the macroion via its distance of closest approach a (i.e., its radius) to the wall (see figure 5 as well) [70]. Two regimes were specifically examined: The strong and weak screening regimes which are now briefly described.

- In the strong screening regime ($\kappa_0 a \gg 1$) † the wall-macroion attractive interaction

† The negative counterions of the positively charged macroions correspond to the coions of the planar substrate. Thereby, electrostatic correlations tend to localize the counterions of the macroions over *its whole surface* in a uniform manner. Hence, as long as the strength of the surface charge density of the oppositely charged substrate is low enough, a finite number of counterions of the macroions should stay in the vicinity of the interface (see figure 5), leading to a surface charge amplification.

† κ_0 stands for the screening strength stemming uniquely from the little ions, see also figure 5.

is exclusively governed by the screening contrast κ_0/κ . ‡ More precisely, it was shown that the contact potential of interaction U_m is merely given by [70]:

$$\beta U_m \simeq 1 - \frac{\kappa}{\kappa_0}. \quad (24)$$

- In the weak screening regime ($\kappa_0 a \ll 1$) and for sufficiently small surface charge density ($\frac{\kappa b}{2Z_m} \gg 1$), the reduced electric field § at contact follows this simple law [70]:

$$E^*(a) \simeq -\frac{\kappa b}{2Z_m} \left(1 - \frac{\kappa_0^2}{\kappa^2}\right) \kappa a. \quad (25)$$

This equation (25) tells us that surface charge amplification is increasing with growing colloidal particle size a and increasing Gouy-Chapman length b (i.e., decreasing σ_s).

4. Image charges in spherical geometry

In a typical experimental setup, the dielectric constant of a macroion is rather low ($\varepsilon_m \approx 2 - 5$) which is much smaller than that of its embedding solvent (e. g., for water $\varepsilon_{\text{solvent}} \approx 80$) leading to a *high dielectric contrast*, $\Delta_\varepsilon \equiv \frac{\varepsilon_{\text{solvent}} - \varepsilon_m}{\varepsilon_{\text{solvent}} + \varepsilon_m}$, at the interface. It turns out that for a perfect *planar* substrate (which can be envisioned as a colloid of vanishing curvature), there is an elegant analytical solution for the electric field. More precisely, the electric field generated by the induced surface charge at the interface positioned at $z = 0$ (due to the presence of a point-like ion of charge q located at $z = \ell$) can be exactly obtained by a “fictive” point-like charge $q_{im} = \Delta_\varepsilon q$ located at the mirror position $z = -\ell$ [71]. This feature corresponds to the so-called method of *image charges*. The inclusion of such image forces for the case of an electrolyte close to a planar dielectric interface was studied in the past by computer simulations [72, 73, 74, 56], integral equation formalisms [75, 76], mean-field [77, 68, 78, 79, 80] and strong-coupling [56] theories. As far as the cylindrical case [81, 82, 83] is concerned, there is no simple “image charge” picture.

The problem of the dielectric discontinuity in *spherical* geometry is, already at the level of a single ion interacting with a dielectric (neutral) sphere, considerably more complicated than its planar counterpart. Indeed, if we want to reformulate the problem in terms of image charges, one would need an *infinite* number of image charges, thus making its usage much less attractive than in the planar case. Due to this difficulty, the problem of image charges in spherical geometry is sparsely studied in soft matter. Nevertheless, twenty years ago, Linse studied the counterion distribution with image forces around spherical charged micelles by means of Monte Carlo simulations [84]. In his work [84], Linse used a *two-image* charge approximation instead of the full continuous image charge distribution. The conclusions of his study remain qualitatively correct.

‡ κ stands for the total screening strength stemming from all the ions present in the solution (also including the macroions), see also figure 5.

§ The reduced electric field is defined as $E^*(z) \equiv -(b/2)e \frac{d\psi(z)}{dz}$ such that at the interface $z = 0$ we have $E^*(0) = -1$.

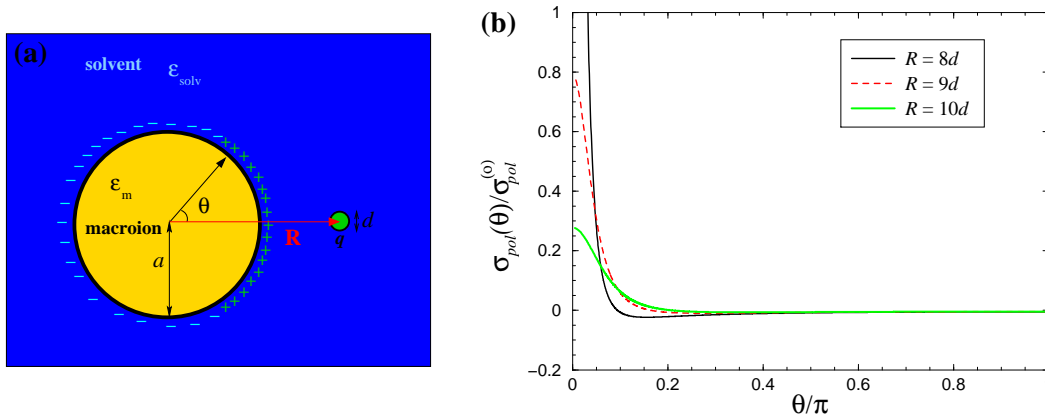


Figure 6. (a) Model for a dielectric sphere (colloid) of dielectric constant ε_m embedded in an infinite medium (the solvent) characterized by a different dielectric constant ε_{solv} . A test positive charge (q) is located near the boundary outside the spherical particle at a radial distance R . The resulting induced surface polarization charges are also illustrated for the case where $\varepsilon_{solv} > \varepsilon_m$. Note that the global induced net charge vanishes. This is a two-dimensional representation of the three-dimensional system. (b) Polar profiles, as obtained from equation (26), of the surface density of polarization charge $\sigma_{pol}^{(sph)}(\theta)$ in units of $\sigma_{pol}^{(0)} = \frac{q}{4\pi\varepsilon_{solv}d^2}$ for different radial distances R of the test charge q with $\varepsilon_{solv} = 80$, $\varepsilon_m = 2$ and $a = 7.5d$.

The dielectric response of a dipolar fluid confined to a spherical cavity was recently addressed by Blaak and Hansen using MD simulations [85].

In the field of image forces in spherical geometry, exact results for the electrostatics of an ion interacting with a dielectric sphere (see figure 6 for the model geometry) were reported [86]. Furthermore, Monte Carlo simulations were performed to elucidate the behavior of an electrolyte near a spherical macroion at finite dielectric contrast, where image forces are properly taken into account [86]. The main results are as follows [86]:

- *Single ion:* A compact and exact analytical expression has been derived for the polar profile of the induced surface charge, and it reads:

$$\sigma_{pol}(\theta) = \frac{q(\varepsilon_{solv} - \varepsilon_m)}{4\pi\varepsilon_{solv}R^2} \sum_{l=1}^{\infty} \left(\frac{a}{R}\right)^{l-1} \frac{(2l+1)l}{\varepsilon_{solv}(l+1) + \varepsilon_m l} P_l(\cos\theta), \quad (26)$$

where q is a test ion at a radial distance R (see figure 6) and P_l designates the Legendre polynomials of order l . The *strength* as well as the *range* of image forces in spherical geometry are considerably smaller than at vanishing curvature, due to *auto-screening*.

- *Electrolyte:* For aqueous monovalent ions the (effective) image force is basically equal to the *self-image* one (i.e., the interaction between an ion and its own image). However, when dealing with multivalent counterions, the *lateral* image-counterion correlations can significantly affect the (local) counterion density and, as a major effect, they *screen* the self-image repulsion. Upon adding salt, it was shown that

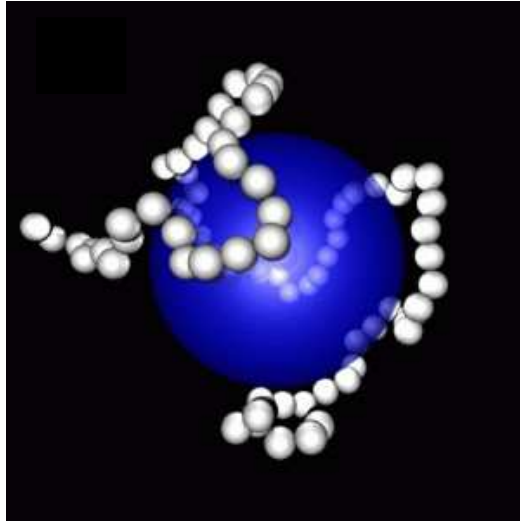


Figure 7. A computer simulation snapshot of PE-colloid complexation (tennis ball-like conformation) [91].

the strength of the image forces induced by the *coions* is marginal. Besides, overcharging is robust against image forces.

Very recently, Reščič and Linse extended [87] the one-colloid problem to the two-colloid interaction problem with dielectric discontinuity. Using a cylindrical cell model and MC simulations, they found (i) weaker counterion accumulation at the macroion's surfaces, (ii) stronger effective repulsion at moderate Coulomb coupling, and (iii) a less attractive effective force at strong Coulomb coupling. These findings are fully consistent with the one-colloid features just discussed above.

5. Polyelectrolyte adsorption and multilayers

Polyelectrolytes (PEs) are polymers containing a variable (usually large) amount of ionizable monomer along the chemical backbone. Once dissolved in a suitable polar solvent such as water, the ion pairs dissociate by creating a charged chain with floating counterions. PEs represent a broad and interesting class of materials that have attracted an increasing attention in the scientific community. PEs have applications in modern technology as well as biology, since virtually all proteins, as well as DNA, are charged. The adsorption of PEs onto surfaces is an important process, since they modify the physico-chemical properties of the surface. From a theoretical point of view, charged polymers (in bulk or adsorbed) are much less understood [88, 89] than neutral ones [90]. One of the main difficulties is the addition of new length scales set by the tremendous long-ranged Coulomb interaction. Hence, the study of adsorption of PEs is motivated by fundamental aspects as well as practical ones.

5.1. Polyelectrolyte-colloid complexation

5.1.1. Oppositely charged spherical substrates The works related to the interaction between PEs and *oppositely* charged spheres are here briefly reviewed.† The complexation of flexible PEs with oppositely charged macroions is a relevant process in biology [94]. For instance a nucleosome can be seen as an electrostatic binding between DNA and histone proteins, where the latter can be envisioned as charged spheres.‡ Many theoreticians [95, 96, 97, 98, 99, 100, 101, 102, 92, 103, 104, 105] have investigated these types of objects to understand the electrostatics governing those structures. Two very relevant results are: (i) the possible overcharging of the sphere by the long PE and (ii) a strong wrapping of the PE about the sphere (see figure 7 for an example). A considerable effort was also provided by the simulators [106, 107, 108, 109, 110, 111, 112, 113, 114, 115, 116, 91, 117] these last twelve years. Some relevant findings in this field can be summarized as follows:

- *The effect of chain stiffness*, which was first systematically studied by Wallin and Linse [106] by MC simulations, is an important key controlling the PE adsorption. They showed that the lower the chain stiffness, the higher the PE adsorption and, concomitantly, the overcharging of the charged sphere by the PE. Stoll and Chodanowski [114], using MC simulation as well but with Yukawa potentials, showed that upon increasing the chain stiffness, *solenoid* conformations are obtained as predicted analytically by Nguyen and Shklovskii [101].
- *The effect of chain length* was also addressed (by means of computer simulations) in the past [108, 112, 113, 115]. For large chain/sphere size ratio, Chodanowski and Stoll [112] found, for fully flexible chains, that only a marginal portion of the PE gets adsorbed to the sphere, and the rest of the chain consists of extended tails. At “moderate” chain/sphere size ratio [112], they found a strong PE collapse into a tennis-ball like structure (as illustrated in figure 7). Considering *both* the effects of chain length and the chain stiffness, Akinchina and Linse [115] reported a rich phase behavior: Tennis-ball like, solenoid, multiloop (also called rosette [94]), single loop, as well as “U”-shaped conformations. Note, that there is remarkable agreement with the rosette structure found theoretically by Schiessel et al. [118].
- The effect of the *discrete* nature of the protein charge distribution was addressed by Carlsson et al. [119]. In their MC simulations [119], they found that complexation can be stronger with a discrete protein charge distribution (in agreement with the ideas discussed in 2.3).
- *Multisphere* complexation involving many charged spheres bridged via oppositely charged PEs were investigated by Jonsson and Linse [110, 111] by means of MC simulations. The effect of linear chain charge density, chain length, and macroion

† The reader can also look at recent reviews [92, 93] on this field for more details.

‡ We are aware that this assumption is at best a caricature of a real system (provided that non-specific interactions are dominant). Nonetheless, from an electrostatic viewpoint, we think that the qualitative features should be captured.

charge valency was addressed in Ref. [110]. Interestingly, at prescribed PE linear charge density, the authors found that complexation gets stronger upon increasing the chain length [110]. The effect of chain flexibility was studied in [111], and it was found that the macroion arrangement gradually becomes more linear and ordered along the (long) chain when its stiffness is increased.

5.1.2. Like-charge complexation Whereas many studies have been devoted for the case of chain-sphere complexation where the two charged bodies are oppositely charged, as we just saw, much less is known concerning the problem of *like-charge sphere-PE complexation*.

In [120, 121], the complexation between a sphere and a long flexible PE (*both negatively charged*) was discussed. Whereas like-charge attraction in the strong Coulomb coupling limit is expected (and therefore complexation too), new and rather unexpected chain conformations are reported. Different coupling regimes as well as the influence of the linear charge density, f , of the PE chain were considered in [121]. The relevant conclusions are as follows:

- At strong coupling the PE chain is always adsorbed in a *flat* structure, whose conformation strongly depends on f . At high f , the conformation consists of densely packed monomers following a Hamiltonian-walk. Upon reducing f the chain tends to spread more and more over the particle surface. These findings could have some relevance for organic solutions.
- Under *aqueous* conditions, complexation can be obtained with multivalent counterions and for high enough values of f . In contrast to the strong coupling case, the formation of *loops* is reported.

5.2. Polyelectrolyte adsorption at planar surfaces

The reader who wants to know a detailed account of the field of PE adsorption at surfaces is invited to consult the recent reviews of Netz and Andelamn [122] and of Dobrynin and Rubinstein [123]. In this part, one would like to propose some basic ideas and features supported by MC simulations about the adsorption of highly charged polyelectrolytes onto oppositely charged *planar* surfaces in a salt-free environment [124, 125, 126]. Flexible [124, 125] as well as rod-like [126] PEs are now discussed.

5.2.1. Role of entropy There is a simple and clear entropic mechanism that influences *multi-polymer-chain* adsorption that is going to be pointed out first. It can be best understood by recalling the *counterion release* effect: The adsorption process of *one* polyion of valence Z typically leads to the release into solution of Z (initially adsorbed) surface monovalent counterions, which is “electrostatically invariant” but entropically (highly) favorable. *This very same effect is also the reason why longer chains can better adsorb at a prescribed monomer density.* Indeed, at prescribed monomer density,

increasing the chain length N_m † involves decreasing the the number of chains. Thereby, the resulting (bulk) entropy stemming from the PE chains becomes reduced accordingly. This entropic mechanism linked to the chain length at prescribed monomer density is henceforth referred to as: *polymerization induced adsorption*.

5.2.2. Flexible chains [124]

When *no* image forces are present (i.e., $\Delta_\epsilon = 0$), it was found that the monomer density profile, $n(z)$, decays monotonically for very short chains even near contact, see figure 8(a). Longer chains experience a short-ranged repulsion in the vicinity of the charged wall ($z \lesssim d$) due to *chain-entropy* effects. ‡

When *image forces* come into play, (partial) monomer desorption sets in, whose strength increases with growing chain length N_m . This feature is due to the repulsive image-chain interaction that scales like N_m^2 , whereas the attractive Wigner crystal correlations§ scales only like $N_m^{3/2}$.

The fraction of charge $\sigma^*(z)$ of the fluid as a function of monomer-wall separation, z , is another interesting quantity to characterize the adsorption behavior. At $\Delta_\epsilon = 0$, overcharging [as signaled by $\sigma^*(z) > 1$] occurs as soon as chains are longer than dimers, see figure 4(a) in [124]. In the presence of image forces, the strength of the overcharging is nearly identical to that obtained without image forces at $\Delta_\epsilon = 0$ (compare with figure 4(a) in Ref. [125]). Thereby, the main effect of image charges is (i) to decrease the fraction of charge $\sigma^*(z)$ near contact ($z \lesssim 1.2a$) upon growing N_m and (ii) to (slightly) shift the position of the maximum of $\sigma^*(z)$ to larger z .

5.2.3. Rigid chains [126]

Dimers exhibit a monotonic behavior for $n(z)$ that is similar to point-like ions. For longer chains there exists a small monomer depletion near the charged wall for an *intermediate* regime of N_m , see figure 8(a). At high enough N_m , $n(z)$ reveals again a monotonic behavior, see figure 1(a) in Ref. [126]. This interesting effect is the result of two antagonistic *entropy*-driving forces, namely, (i) chain-entropy and (ii) polymerization induced adsorption. Electrostatic chain-chain correlations, whose strength grows in a non-trivial way with N_m ,|| favor also chain adsorption. Figure 8(a) clearly shows that the adsorption of rigid PEs is much stronger than that of flexible

† Rigorously, N_m represents the number of monomers per chain corresponding experimentally to the polymerization degree.

‡ The chain-entropy effect here is merely due to the much lower number of available conformations in the adsorbed state. It has to be distinguished from that previously discussed in 5.2.1.

§ When charged polymers are adsorbed on the surface, they also tend to build a Wigner crystal due to the strong mutual Coulomb inter-chain repulsion. The higher the chain length N_m (i.e., the length of the chain) the stronger the effect. At prescribed reduced surface charge density σ_s and monomer concentration, this leads to a 2D plasma term (i.e., interchain repulsion reduced by thermal energy) that roughly varies like $N_m^{3/2}$, as is the case for point-like multivalent ions.

|| Due to the strong extension of the chain, it is no longer suitable to use the point-like and/or spherical polyion picture leading to the WC term in $N_m^{3/2}$.

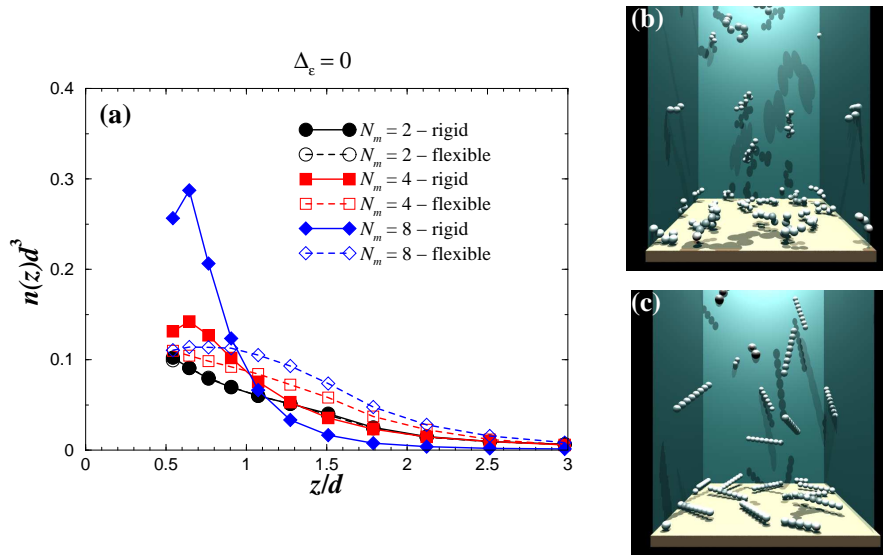


Figure 8. (a) Profiles of the monomer density $n(z)$ for various chain length N_m : *flexible* vs *rigid* chains [126]. Snapshots at $N_m = 8$ for (b) flexible and (c) rigid chains.

ones. This feature is also detectable in the snapshots, see figure 8(b) and 8(c).

Upon polarizing the interface, it is found that the degree of adsorption is considerably reduced. Nonetheless, a comparison with the flexible case [125] shows that the values at contact at finite Δ_ϵ are quite similar.

5.2.4. Summary To sum up, MC simulations [124, 125, 126] show us that:

- Without a dielectric discontinuity ($\Delta_\epsilon = 0$), *flexible* PE chains experience short-ranged repulsion near the charged substrate due to chain-entropy effects. In contrast, *rigid* PE chains are more strongly adsorbed (due to a weaker loss of chain-entropy) and, when long enough, experience a purely effective attraction.
- Image forces lower the degree of adsorption for flexible and rigid PE chains. However, the overcharging of the substrate by the PEs is robust (irrespective of the chain flexibility) against image forces.

5.3. Polyelectrolyte multilayering

PE multilayer thin films are often obtained using a so-called layer-by-layer deposition technique [127, 128]: A (say negatively) charged substrate is alternatively exposed to a polycation (PC) solution and a polyanion (PA) one. This method and the resulting materials have a fantastic potential of application in technology, e. g., biosensing [129], catalysis [130], nonlinear optical devices [131], nanoparticle coating [132], etc.

From the theoretical side the literature is rather poor. However, a few analytical works about PE multilayers on charged planar surfaces based on different levels of approximation are available [133, 134, 135]. Solis and Olvera de la Cruz considered the conditions under which the spontaneous formation of polyelectrolyte layered structures

can be induced by a charged wall [133]. Based on Debye-Hückel approximations for the electrostatic interactions, but including some lateral correlations by the consideration of given adsorbed PE structures, Netz and Joanny [134] found a remarkable stability of the (semi-flexible) PE multilayers supported by scaling laws. For weakly charged flexible polyelectrolytes at high ionic strength, qualitative agreements between theory [135], also based on scaling laws, and experimental observations [136] (such as the predicted thickness and net charge of the PE multilayer) were achieved. More recently, Shafir and Andelman, using mean-field theory, pointed out the relevant role of a specific strong short-range interaction between PAs and PCs.

A tremendous difficulty in PE multilayering is the strong electrostatic correlations between PCs and PAs, which are hard to be satisfactorily taken into account in (modified) mean-field theories. In this respect, computer simulations are of great help. The first simulation model for PE multilayering was developed in [91]. Later Panchagnula et al. performed similar computer simulations [137], where the dynamical aspect was more emphasized. Several types of substrate geometry were considered, from spherical particles [91, 137, 138] to planar substrates [139, 140] via cylindrical ones [141]. Relevant simulation findings for spherical [91] and planar substrates [139] are going to be described.

5.3.1. Polyelectrolyte multilayering at spherical substrates From the study in [91] concerning substrates with finite radii (i. e., charged spheres), one has learned that *non-electrostatic* forces are required to obtain (true) PE multilayers. More precisely, by introducing a (additional) *short-range* van der Waals-like attraction (whose strength is characterized by its value at contact, χ_{vdw} , in units of $k_B T$) between the substrate's surface and the (monomers of the) oppositely charged chains. The PE structure results then from a complicated interplay between: (i) PC-PA strong attraction (favoring a collapse into a compact globular state) and (ii) PE-substrate correlations (favoring *flat* adsorption and *wrapping* † around the sphere). Briefly, the main findings in [91] are as follows:

- Flat *bilayer*-structures, involving two long oppositely charged chains, set in only for large enough χ_{vdw} . At low χ_{vdw} , the strong driving PA-PC force leads to PE globular structures, see figure 9.
- Stable and flat multilayers are only obtainable at large enough χ_{vdw} . In a purely electrostatic regime ($\chi_{vdw} = 0$) PE globules are formed preventing a uniform coverage of the surface, see figure 10.
- Short chains are not suitable candidates for PE multilayers, due to (i) the weaker effect of polymerization adsorption and (ii) reduced chain-chain correlations.

† Note that the wrapping from the chain(s) around the colloid is peculiar to spherical substrates. Besides it should be reminded that wrapping is also governed by the repulsive interaction between the turns of a chain [35].

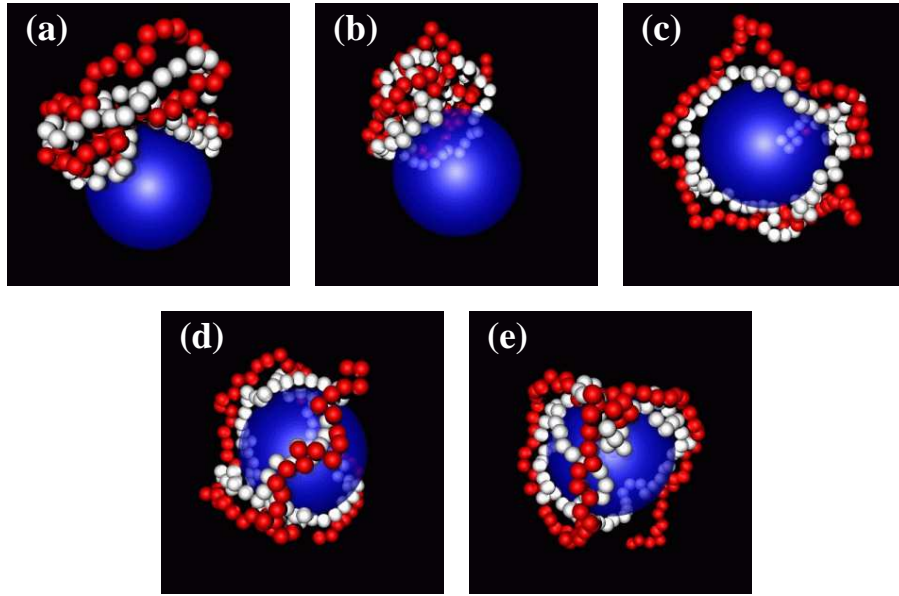


Figure 9. Typical configurations for one PC (in white) and one PA (in red) adsorbed onto the negatively charged colloid at different χ_{vdw} -couplings. (a) $\chi_{vdw} = 0$ (b) $\chi_{vdw} = 1$ (c) $\chi_{vdw} = 2$ (d) $\chi_{vdw} = 3$ (e) $\chi_{vdw} = 5$. Note the remarkable structural change occurring at $\chi_{vdw} = 2$. The small univalent counterions (anions and cations) are omitted for clarity.

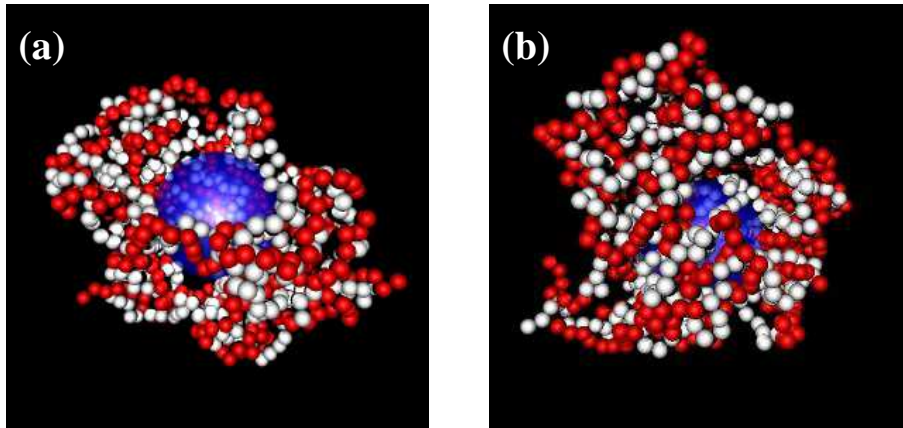


Figure 10. Typical equilibrium configurations for 12 PEs (6 PCs in white and 6 PAs in red) adsorbed onto the negatively charged colloid at different χ_{vdw} -couplings. The little counterions (anions and cations) are omitted for clarity. (a) $\chi_{vdw} = 0$ (b) $\chi_{vdw} = 3$.

5.3.2. Planar substrates PE multilayering onto planar substrates were investigated in [139, 142, 140]. The zero-curvature case differs qualitatively from the spherical one. First the intrinsic electric field is higher in the former case †. Secondly the chain-wrapping is no-longer present at zero curvature. Consequently at given surface charge density, we expect a stronger PE-layering. The important results can be formulated as follows:

† At zero curvature we have $\psi \sim r$ in contrast to finite curvature where $\psi \sim 1/r$

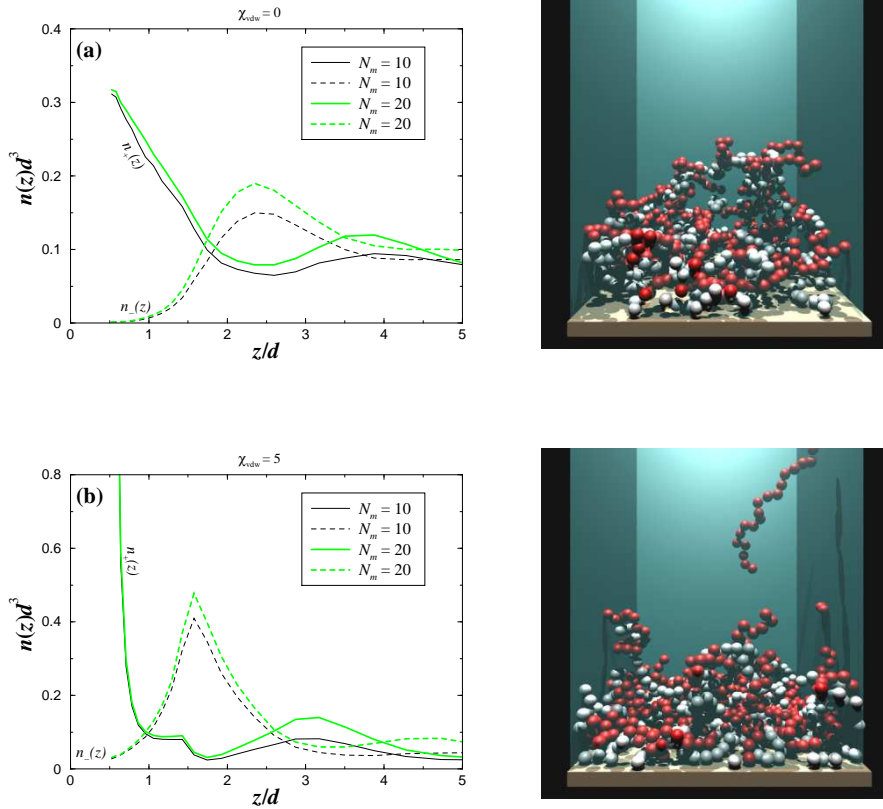


Figure 11. Profiles of monomer density $n_{\pm}(z)$ for oppositely charged PEs adsorbed onto a negatively charged planar substrate. χ_{vdw} -couplings. (a) $\chi_{vdw} = 0$ (b) $\chi_{vdw} = 5$ [139]. The snapshots shown correspond to chain length $N_m = 20$.

- As with for spherical substrates, the relevance of short-ranged non-electrostatic forces is also demonstrated here, see figure 11. Flat multilayers can not be achieved with solely electrostatic forces.
- The formation of islands (i.e., clusters of PC-PA chains) onto the substrate are reported [139] and qualitatively confirm the experimental observations of the early stages of PE deposition (one or two bilayers) [143, 144].

6. Confined crystalline colloids

It is well known from solid state studies that strongly confined (i.e., quasi two-dimensional) systems exhibit properties and a phase behavior that may drastically differ from those in the bulk [145]. This feature is also vivid in colloidal systems, and those materials represent ideal model systems to analyze (experimentally as well as theoretically) and understand confinement effects on a mesoscopic scale corresponding to the interparticle distance. Using external fields, a colloidal system can be prepared in a controlled way into prescribed equilibrium and non-equilibrium states [146]. For instance, in equilibrium, solidification near interfaces (provided by a substrate or a large

“impurity”) can occur under thermodynamic conditions where the bulk is still fluid (so-called prefreezing). In non-equilibrium, a wall may act as a center of heterogeneous nucleation (favored by the excess surface-energy already offered by the wall/nucleus interface) and initiate crystal growth. Most of our experimental knowledge of freezing in a confining slit-like geometry is based on real-space measurements of mesoscopic model systems such as charged colloidal suspensions between glass plates [147, 148].

In this section, different relevant achievements in the field of confined charged colloidal crystals are discussed.

6.1. Two-dimensional dipolar mixtures

Two-dimensional colloidal systems can be achieved for instance via sedimentation and trapping at the air/water interface [149, 150]. At strong external field, all the dipolar moments are aligned in the direction of the applied external field, leading to a purely repulsive pair interaction that scales like:

$$V_{dip}(r) \propto \frac{m_1 m_2}{r^3}, \quad (27)$$

where m_1 and m_2 stand for the induced dipolar moments of the particles 1 and 2, respectively. †

Whereas the one-component situation trivially yields a triangular lattice, the *binary mixture* situation provides a very rich phase behavior [152]. This feature can be conveniently exploited for potential technological applications: optical band-gap materials (so-called photonic crystals) [153], molecular sieves [154], nano-filters with prescribed porosity [155], etc. There have been recent advances in this field that are going to be concisely explained here.

Two dimensional binary mixtures made up of two types of dipolar particles [(i) big particles with a large dipolar moment (species A) and (ii) small particles with a small dipolar moment (species B)] were investigated experimentally [150]. The corresponding setup and a representative snapshot of the microstructure are shown in figure 12. A remarkable feature is the stability of the square phase at strong dipolar asymmetry ($m_B/m_A \approx 10\%$).

On the theoretical side, the phase behavior of such a binary dipolar mixture at zero temperature was studied using lattice sums [152]. The relevant reduced parameters are (i) the reduced dipolar moment $m = m_B/m_A$ and (ii) the composition $X = n_B/(n_A + n_B)$. The resulting phase diagram is shown in figure 13. The main results are as follows:

- The phase diagram qualitatively differs from that of hard disks [156]. For low dipolar asymmetry $m \gtrsim 0.5$ a stable mixture $\mathbf{T}(AB_2)$ sets in (see figure 13) in

† Note that in the experimental situations, one has often to deal with *magnetic* colloidal particles (so called ferrofluids). However *electric* dipoles are also realizable [151]. This being said, regardless of the nature of dipolar moment (i.e., magnetic or electric), the same pair interaction (27) prevails. Hence results on (super)magnetic particles enter also adequately in the scope of this review.

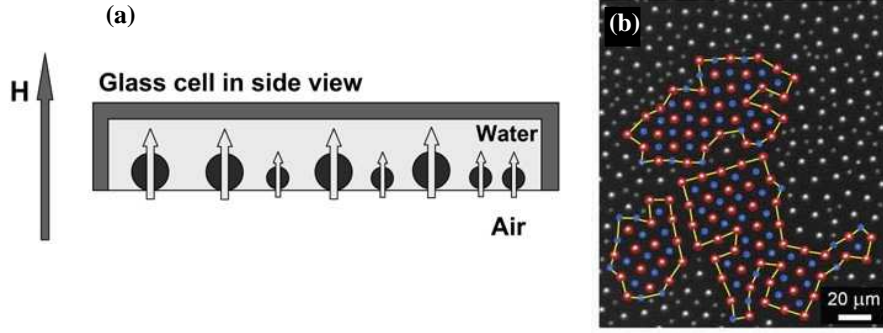


Figure 12. (a) Super-paramagnetic colloidal particles confined at a water/air interface due to gravity. An external magnetic field H perpendicular to the interface induces a magnetic moment \vec{m} in each bead leading to a repulsive dipolar interaction, see equation (27). (b) Micrograph showing three touching square-latticed grains at low reduced temperature with a global composition $X = n_B/(n_B + n_A) \approx 45\%$ [with n_A and n_B standing for the area density of the big and small particles, respectively] and a reduced moment $m_B/m_A \approx 10\%$. Data taken from [150].

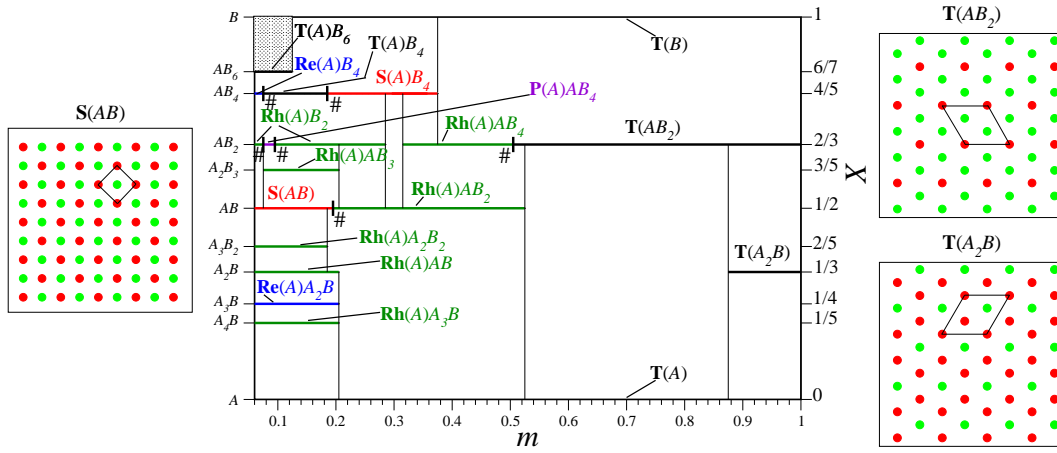


Figure 13. The phase diagram in the (m, X) -plane at $T = 0$. Three important phases are shown: $\mathbf{S}(AB)$, $\mathbf{T}(A_2B)$ and $\mathbf{T}(AB_2)$. The reader can find more details about the other structures in [152]. Data taken from [152].

contrast to the case of hard-disk mixtures where *no* mixture is predicted at low size asymmetry [156]. The stability of this phase $\mathbf{T}(AB_2)$ was also reported in molecular dynamics simulations [157]. At even smaller dipolar asymmetry $m \gtrsim 0.88$, an additional (globally triangular) phase mixture $\mathbf{T}(A_2B)$ is stable, see figure 13.

- The stability of the square phase $\mathbf{S}(AB)$ (see figure 13) is in good qualitative agreement with the experimental findings in [150], where the dominance of the square phase is also reported (see figure 12) as previously mentioned.

6.2. Crystalline colloidal bilayers

Crystalline bilayers made up of charged particles have been intensively studied these last years in the soft matter colloid community [158, 159] as well as in the solid state physics (classical [160, 161, 162, 163, 164] and non-classical electrons [165, 166, 167]) and dusty plasma communities [168, 169].

The effective interaction between these constitutive mesoscopic macroions is neither hard-sphere like nor purely Coulombic, but it is rather described by an intermediate screened Coulomb [also called Yukawa or DLVO (Derjaguin-Landau-Verwey-Overbeek) [170, 171]] due to the screening mediated by the additional microions present in the system. The screening strength can be tuned by varying the microion concentration: For colloidal systems, salt ions can be conveniently added to the aqueous suspension; The dusty plasma, on the other hand, consists of electrons and impurity ions.

6.2.1. Equilibrium The *equilibrium* phase diagram at zero temperature of crystalline bilayers was investigated theoretically in [158]. The constitutive (point-like) particles interact via a Yukawa pair potential of the form

$$V_{yuk}(r) = V_0 \frac{\exp(-\kappa r)}{\kappa r}, \quad (28)$$

where V_0 sets the energy scale.† The choice of this potential is motivated by the experimental model systems described above. The crystalline bilayer consists of two (identical) layers containing in total N particles in the (x, y) plane. The corresponding (total) surface density ρ is then given by N/A , with A being the (macroscopic) layer area. The distance D , separating the two layers in the z -direction, is prescribed by an (implicit) external potential confining the system.

The zero-temperature phase behavior is fully determined by two dimensionless parameters, namely the reduced layer density, $\eta = \rho D^2/2$, and the reduced screening strength, $\lambda = \kappa D$. Using a straightforward lattice sum technique, the phase diagram was calculated for arbitrary λ and η , see figure 14.‡ The most interesting findings [158] are as follows:

- Whereas the two known extreme limits of zero [163, 162, 160] and infinite [172, 173, 174] screening strength λ are recovered by lattice sum calculations [158],

† Note that in the ground state, i.e. at rigorously zero temperature, the value of V_0 is irrelevant. Nonetheless in experimental situations, the energy amplitude $V_0 = Z^2 \kappa \frac{\exp(2\kappa R)}{\varepsilon(1+\kappa R)^2}$ scales like the square of the charge Z of the particles with a physical hard core radius R reduced by the dielectric constant ε of the solvent ($\varepsilon = 1$ for the dusty plasma). For a charged colloids, Z is typically of the order of 100 – 100 000 elementary charges such that $V(r = d)$ can be much larger than $k_B T$ at interparticle distance (d), justifying formally our zero-temperature calculations.

‡ Note that the ground state at vanishing screening $\lambda \rightarrow 0$ corresponds always to bilayers. Indeed, two equally charged walls do *not* generate any electric field within the slit, and consequently they do not alter the stable Wigner crystal structure obtained at any other surface charge density (including neutral walls). Thereby, if one considers the special case of two walls corresponding to neutralizing backgrounds, the ground state is always a bilayer. At finite screening $\lambda \neq 0$, however, the situation is more complicated, and multilayers (i.e., beyond bilayers) are stable at high enough density η .

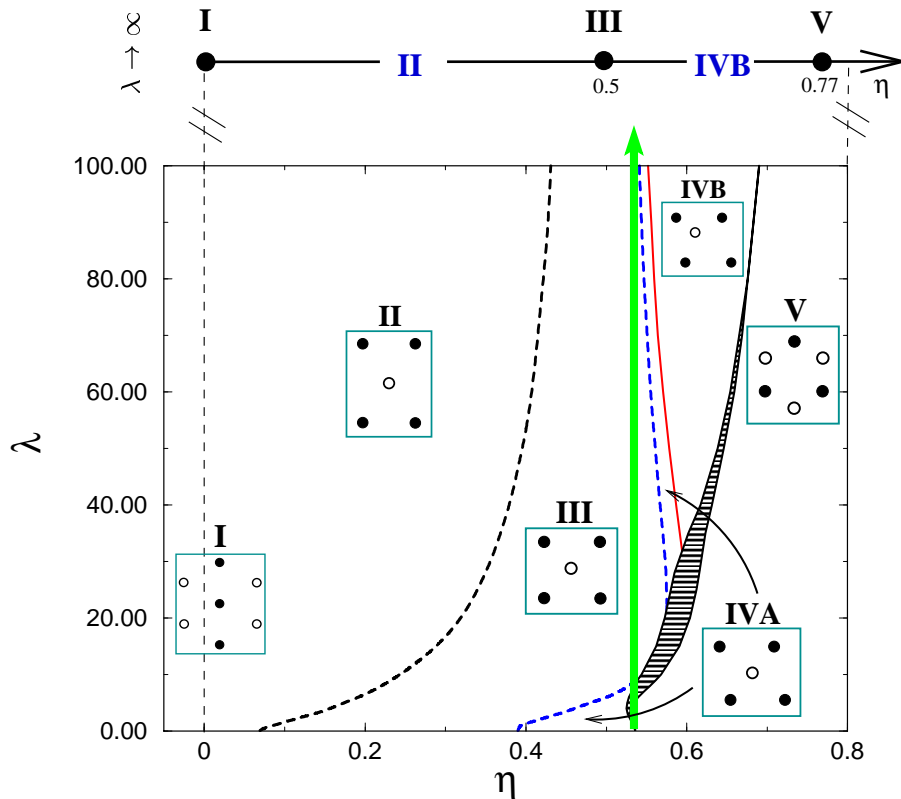


Figure 14. The hard sphere limit $\lambda \rightarrow \infty$ is sketched on top. The dashed (solid) lines denote continuous (discontinuous) transitions. The filled region corresponds to the coexistence domain of phases IV and V. The vertical arrow indicates the *double reentrant* behavior of phase IVB. The insets show the lattice geometries, where the filled (open) circles correspond to the lower (upper) layer.

it is demonstrated that, at intermediate λ , the phase behavior is strikingly different from a simple interpolation between these two limits. First, there is a first-order coexistence between two different staggered rhombic lattices (IVB and IVB in figure 14) differing in their relative shift of the two unit cells. Second, the staggered rhombic phase IVB exhibits a novel reentrant effect for fixed density and varied screening length, see figure 14. Depending on the density, the reentrant transition can proceed via a staggered square III or a staggered triangular solid V including even a *double reentrant transition* of the rhombic phase IVB, see figure 14.

- A comparative study [159] of the phase behavior of highly charged colloidal spheres in a confined wedge geometry reveals semi-quantitative agreement between theory and experiment.

6.2.2. Non-equilibrium The *non-equilibrium* case[†] at finite temperature as driven by a linear shear flow has been addressed in [175, 176]. The steady state developed under shear as well as the relaxation back to equilibrium after cessation of shear were analyzed with the help of non-equilibrium Brownian dynamics. The pertinent results are:

- For increasing shear rates, the following steady states are reported: First, up to a threshold of the shear rate, there is a static solid which is elastically sheared. Then, at higher shear rates the crystalline bilayer melts, and even higher shear rates lead to a reentrant solid stratified in the shear direction.
- After instantaneous cessation of shear, a nonmonotonic behavior of the typical relaxation time is found. In particular, application of high shear rates accelerates the relaxation back to equilibrium since shear-induced ordering facilitates the growth of the equilibrium crystal.
- The orientation of a crystalline bilayer can be tuned at wish upon applying a (strong) shear rate in the desired direction and subsequently letting the system relax.

7. Conclusions

Various electrostatic effects in soft matter have been discussed. Generally speaking, charged systems are fascinating because they simultaneously involve short-ranged excluded volume effects (as soon as the latter are properly taken into account) already present in neutral systems, and additionally the long-ranged Coulomb interaction. The latter constitutes a formidable theoretical challenge.

In terms of similarities with classical solid state physics and (elementary) quantum chemistry, two striking analogies were identified: (i) The overcharging occurring at a sphere reduces to the old Thomson problem; (ii) The ground state of two spherical macroions is ionized, with the degree of ionization (and therefore the attraction strength) growing with the *difference in surface charge density* between the two macroions. This behavior is highly reminiscent of the (molecular) ionic bonding [177] where the *difference in electronegativity* between the two atoms governs its stability.

Excluded volume effects are equally important to fully understand phenomena like overcharging (i.e., surface charge reversal) and surface charge amplification. For overcharging, the counterion layer can reach a high ordering when the local packing fraction is raised, by simply increasing the size of the adsorbed counterions.

Image forces turn out to be systematically short-ranged. Their effects are only vivid close to the substrate at distances corresponding roughly to the linear size of

[†] The starting unsheared configuration corresponds to a staggered square lattice with a reduced surface particle density $\eta = 0.24$ and a reduced screening strength $\lambda = 2.5$. Two walls are present to ensure the confinement. To this end, screened Coulomb and short-ranged (of the Lennard-Jones type) repulsive potentials were tested, and it was found that our results are marginally sensitive to the choice of the repulsive wall-particle interaction.

the microions[†] (counterions and/or charged monomers). As far as the adsorption of polyelectrolytes is concerned, there are two important driving forces that act concomitantly: (i) The polymerization-induced adsorption that works like the principle of counterion release (so *entropy* based) and (ii) purely electrostatic lateral correlations (reminiscent of the classical Wigner crystal).

Confined colloidal crystals seem to be now pretty well understood up to bilayers. There is presently some experimental [178, 179] and simulational [180] evidence that, upon increasing the projected surface particle density, the transition from two-layer to three-layer structures involve four (and even more) layered crystalline structures. This is a problem that needs an urgent and clear understanding.

On a more “material/engineering” level, multilayered structures can apparently also be experimentally obtained by combining oppositely charged colloids/micelles [181], instead of polyelectrolytes. To explore this new field, a considerable theoretical effort would be needed to identify the parameters phase space (such as salt concentration, charges of the colloids and the substrates, particle size etc.) allowing the onset of such structures without strong clustering.

Acknowledgments

The author is grateful to C. Holm, K. Kremer, H. Löwen, and M. Lozada-Cassou who are closely involved in jointly authored publications covered in this review.

References

- [1] E. Madelung, *Phys. Z.* **19**, 542 (1918).
- [2] P. P. Ewald, *Ann. Phys.* **64**, 253 (1921).
- [3] R. P. Feynman, R. B. Leighton, and M. Sands, in *The Feynman Lectures on Physics - Mainly Electromagnetism and Matter*, definitive ed. (Addison-Wesley, Massachusetts, 2006), Vol. 2, Chap. 8: Electrostatic Energy.
- [4] G. L. Gouy, *J. Phys. Radium* **9**, 457 (1910).
- [5] D. L. Chapman, *Philos. Mag.* **25**, 475 (1913).
- [6] P. Debye and E. Hückel, *Phys. Z* **24**, 185 (1923).
- [7] D. Andelman, in *Electrostatic Properties of Membranes: The Poisson-Boltzmann Theory*, Vol. 1 of *Handbook of Biological Physics*, edited by R. Lipowsky and E. Sackman (Elsevier Science, Amsterdam, 1995), Chap. 12.
- [8] J.-P. Hansen and I. R. McDonald, in *Theory of Simple Liquids*, 3rd ed. (Academic, London, 2006), Chap. 4, p. 84.
- [9] D. A. McQuarrie, in *Statistical Mechanics* (Harper & Row, New York, 1976), Chap. 15, p. 345.
- [10] B. I. Shklovskii, *Phys. Rev. E* **60**, 5802 (1999).
- [11] A. G. Moreira and R. R. Netz, *Europhys. Lett.* **52**, 705 (2000).
- [12] R. R. Netz and H. Orland, *Europhys. Lett.* **45**, 726 (1999).
- [13] R. R. Netz and H. Orland, *Eur. Phys. J. E* **1**, 203 (2000).
- [14] B. I. Shklovskii, *Phys. Rev. Lett.* **82**, 3268 (1999).
- [15] L. Bonsall and A. A. Maradudin, *Phys. Rev. B* **15**, 1959 (1977).
- [16] I. Rouzina and V. A. Bloomfield, *J. Chem. Phys.* **100**, 9977 (1996).

[†] The behavior might be less clear for highly charged spherical macroions as adsorbate.

- [17] H. Wennerström, B. Jönsson, and P. Linse, *J. Chem. Phys.* **76**, 4665 (1982).
- [18] G. S. Manning, *J. Chem. Phys.* **51**, 924 (1969).
- [19] M. Lebret and B. H. Zimm, *Biopolymers* **23**, 287 (1984).
- [20] Y. Levin and M. E. Fisher, *Physica A* **225**, 164 (1996).
- [21] B. Jönsson, H. Wennerström, and B. Halle, *J. Phys. Chem.* **84**, 2179 (1980).
- [22] M. Lebret and B. H. Zimm, *Biopolymers* **23**, 271 (1984).
- [23] M. Deserno, C. Holm, and S. May, *Macromolecules* **33**, 199 (2000).
- [24] M. C. Barbosa, M. Deserno, C. Holm, and R. Messina, *Phys. Rev. E* **69**, 051401 (2004).
- [25] P. Linse, *Adv. Polym. Sci.* **185**, 111 (2005).
- [26] A. Esztermann, R. Messina, and H. Löwen, *Europhys. Lett.* **73**, 864 (2006).
- [27] L. Belloni, *Colloids Surf.* **A140**, 227 (1998).
- [28] W. Bu, D. Vaknin, and A. Travesset, *Langmuir* **22**, 5673 (2006).
- [29] E. Trizac and J.-L. Raimbault, *Phys. Rev. E* **60**, 6530 (1999).
- [30] M. Ruela Talingting, U. Voigt, P. Munk, and S. E. Webber, *Macromolecules* **33**, 9612 (2000).
- [31] W. Lin, P. Galletto, and M. Borkovec, *Langmuir* **20**, 7465 (2004).
- [32] R. Messina, C. Holm, and K. Kremer, *Phys. Rev. E* **64**, 021405 (2001).
- [33] J. J. Thomson, *Philos. Mag* **7**, 237 (1904).
- [34] D. J. Wales and S. Ulker, *Phys. Rev. B* **74**, 212101 (2006).
- [35] A. Y. Grosberg, T. T. Nguyen, and B. I. Shklovskii, *Rev. Mod. Phys.* **74**, 329 (2002).
- [36] R. Messina, C. Holm, and K. Kremer, *Phys. Rev. Lett.* **85**, 872 (2000).
- [37] Y. Levin, *Rep. Prog. Phys.* **65**, 1577 (2002).
- [38] Y. Levin and J. J. Arenzon, *Europhys. Lett.* **63**, 415 (2002).
- [39] M. Patra, M. Patriarca, and M. Karttunen, *Phys. Rev. E* **67**, 031402 (2003).
- [40] A. K. Mukherjee, K. S. Schmitz, and L. B. Bhuiyan, *Langmuir* **19**, 9600 (2003).
- [41] N. Grønbech-Jensen, K. M. Beardmore, and P. Pincus, *Physica* **261A**, 74 (1998).
- [42] E. Allahyarov, I. D'Amico, and H. Löwen, *Phys. Rev. Lett.* **81**, 1334 (1998).
- [43] P. Linse and V. Lobaskin, *Phys. Rev. Lett.* **83**, 4208 (1999).
- [44] M. J. Stevens and M. O. Robbins, *Europhys. Lett.* **12**, 81 (1990).
- [45] A. W. C. Lau, D. Levine, and P. Pincus, *Phys. Rev. Lett.* **84**, 4116 (2000).
- [46] N. Grønbech-Jensen, R. J. Mashl, R. F. Bruinsma, and W. M. Gelbart, *Phys. Rev. Lett.* **78**, 2477 (1997).
- [47] B. Y. Ha and A. J. Liu, *Phys. Rev. Lett.* **79**, 1289 (1997).
- [48] A. A. Kornyshev and S. Leikin, *Phys. Rev. Lett.* **82**, 4138 (1999).
- [49] J. J. Arenzon, J. F. Stilck, and Y. Levin, *Eur. Phys. J. B* **12**, 79 (1999).
- [50] A. Naji, A. Arnold, C. Holm, and R. R. Netz, *Europhys. Lett.* **67**, 130 (2004).
- [51] G. Odriozola, F. Jiménez-Ángeles, and M. Lozada-Cassou, *Phys. Rev. Lett.* **97**, 018102 (2006).
- [52] R. Messina, C. Holm, and K. Kremer, *Europhys. Lett.* **51**, 461 (2000).
- [53] A. K. Mukherjee, *J. Phys.: Condens. Matter* **16**, 2907 (2003).
- [54] R. Messina, C. Holm, and K. Kremer, *Eur. Phys. J. E* **4**, 363 (2001).
- [55] R. Messina, *Physica A* **308**, 59 (2002).
- [56] A. G. Moreira and R. R. Netz, *Europhys. Lett.* **57**, 911 (2002).
- [57] D. B. Lukatsky, S. A. Safran, A. W. C. Lau, and P. Pincus, *Europhys. Lett.* **58**, 785 (2002).
- [58] E. Allahyarov, H. Löwen, J. P. Hansen, and A. A. Louis, *Phys. Rev. E* **67**, 051404 (2003).
- [59] M. L. Henle, C. D. Santangelo, D. M. Patel, and P. A. Pincus, *Europhys. Lett.* **66**, 284 (2004).
- [60] P. Taboada-Serrano, S. Yioucoumi, and C. Tsouris, *J. Chem. Phys.* **123**, 054703 (2005).
- [61] K. Qamhie and P. Linse, *J. Chem. Phys.* **123**, 104901 (2005).
- [62] S. Madurga *et al.*, *J. Chem. Phys.* **126**, 234703 (2007).
- [63] J. J. Spitzer, *J. Colloid Interface Sci.* **92**, 198 (1983).
- [64] E. González-Tovar, M. Lozada-Cassou, and D. Henderson, *J. Chem. Phys.* **83**, 361 (1985).
- [65] H. Greberg and R. Kjellander, *J. Chem. Phys.* **108**, 2940 (1998).
- [66] M. Deserno, F. Jiménez-Ángeles, C. Holm, and M. Lozada-Cassou, *J. Phys. Chem. B* **105**, 10983

- (2001).
- [67] R. Messina, E. González-Tovar, M. Lozada-Cassou, and C. Holm, *Europhys. Lett.* **60**, 383 (2002).
 - [68] R. R. Netz, *Phys. Rev. E* **60**, 3174 (1999).
 - [69] P. Gonzáles-Mozuelos and M. Medina-Noyola, *J. Chem. Phys.* **94**, 1480 (1991).
 - [70] R. Messina, *J. Chem. Phys.* **127**, 214901 (2007).
 - [71] J. D. Jackson, *Classical Electrodynamics* (Wiley, New York, 1975).
 - [72] G. M. Torrie, J. P. Valleau, and G. N. Patey, *J. Chem. Phys.* **76**, 4615 (1982).
 - [73] G. M. Torrie, J. P. Valleau, and C. W. Outhwaite, *J. Chem. Phys.* **81**, 6296 (1984).
 - [74] D. Bratko, B. Jönsson, and H. Wennerström, *Chem. Phys. Lett.* **128**, 449 (1986).
 - [75] R. Kjellander and S. Marčelja, *Chem. Phys. Lett.* **112**, 49 (1984).
 - [76] R. Kjellander and S. Marčelja, *J. Chem. Phys.* **82**, 2123 (1985).
 - [77] C. W. Outhwaite and L. B. Bhuiyan, *J. Chem. Soc. Faraday Trans. II* **79**, 707 (1983).
 - [78] H. H. von Grünberg and E. C. Mbamala, *J. Phys. Condens. Matter* **12**, 10349 (2000).
 - [79] P. Sens and J.-F. Joanny, *Phys. Rev. Lett.* **84**, 4862 (2000).
 - [80] L. B. Bhuiyan, C. W. Outhwaite, D. Henderson, and M. Alawneh, *Mol. Phys.* **105**, 1395 (2007).
 - [81] J. Skolnick and M. Fixman, *Macromolecules* **11**, 867 (1978).
 - [82] A. Wynveen and F. Bresme, *J. Chem. Phys.* **124**, 104502 (2006).
 - [83] F. Bresme and A. Wynveen, *J. Chem. Phys.* **126**, 044501 (2007).
 - [84] P. Linse, *J. Phys. Chem.* **90**, 6821 (1986).
 - [85] R. Blaak and J.-P. Hansen, *J. Chem. Phys.* **127**, 214901 (2007).
 - [86] R. Messina, *J. Chem. Phys.* **117**, 11062 (2002).
 - [87] J. Reščič and P. Linse, *J. Chem. Phys.* **129**, 114505 (2008).
 - [88] J.-L. Barrat and J.-F. Joanny, *Adv. Chem. Phys.* **94**, 1 (1996).
 - [89] J. F. Joanny, in *Electrostatic Effects in Soft Matter and Biophysics*, edited by C. Holm, P. Kékicheff, and R. Podgornik (Kluwer Academic Publishers, Netherlands, 2001), Vol. 46, Chap. Scaling description of charged polymers, p. 149.
 - [90] P. G. de Gennes, *Scaling Concepts in Polymer Physics* (Cornell University Press, Ithaca, New York, 1979).
 - [91] R. Messina, C. Holm, and K. Kremer, *Langmuir* **19**, 4473 (2003).
 - [92] R. de Vries and M. C. Stuart, *Current Opinion in Colloid and Interface Science* **11**, 295 (2006).
 - [93] R. Messina, C. Holm, and K. Kremer, *J. Polym. Science: Part B Polym. Phys.* **42**, 3557 (2004).
 - [94] H. Schiessel, *J. Phys.: Condens. Matter* **15**, R699 (2003).
 - [95] F. von Goeler and M. Muthukumar, *J. Chem. Phys.* **100**, 7796 (1994).
 - [96] E. Gurovitch and P. Sens, *Phys. Rev. Lett.* **82**, 339 (1999).
 - [97] E. M. Mateescu, C. Jeppesen, and P. Pincus, *Europhys. Lett.* **46**, 493 (1999).
 - [98] S. Y. Park, R. F. Bruinsma, and W. M. Gelbart, *Europhys. Lett.* **46**, 454 (1999).
 - [99] R. R. Netz and J. F. Joanny, *Macromolecules* **32**, 9026 (1999).
 - [100] K.-K. Kunze and R. R. Netz, *Phys. Rev. Lett.* **85**, 4389 (2000).
 - [101] T. T. Nguyen and B. I. Shklovskii, *Physica A* **293**, 324 (2001).
 - [102] H. Schiessel, *Macromolecules* **36**, 3424 (2003).
 - [103] R. G. Winkler and A. G. Cherstvy, *Phys. Rev. Lett.* **96**, 066103 (2006).
 - [104] A. G. Cherstvy and R. G. Winkler, *J. Chem. Phys.* **125**, 064904 (2007).
 - [105] R. G. Winkler and A. G. Cherstvy, *J. Phys. Chem. B* **111**, 5436 (2007).
 - [106] T. Wallin and P. Linse, *Langmuir* **12**, 305 (1996).
 - [107] T. Wallin and P. Linse, *J. Phys. Chem.* **100**, 17873 (1996).
 - [108] T. Wallin and P. Linse, *J. Phys. Chem. B* **101**, 5506 (1997).
 - [109] C. Y. Kong and M. Muthukumar, *J. Chem. Phys.* **109**, 1522 (1998).
 - [110] M. Jonsson and P. Linse, *J. Chem. Phys.* **115**, 3406 (2001).
 - [111] M. Jonsson and P. Linse, *J. Chem. Phys.* **115**, 10975 (2001).
 - [112] P. Chodanowski and S. Stoll, *Macromolecules* **34**, 2320 (2001).
 - [113] P. Chodanowski and S. Stoll, *J. Chem. Phys.* **115**, 4951 (2001).

- [114] P. Chodanowski and S. Stoll, *Macromolecules* **35**, 9556 (2002).
- [115] A. Akinchina and P. Linse, *Macromolecules* **35**, 5183 (2002).
- [116] J. Dzubiella, A. G. Moreira, and P. A. Pincus, *Macromolecules* **36**, 1741 (2003).
- [117] P. K. Maiti and B. Bagchi, *Nano Letters* **6**, 2478 (2006).
- [118] H. Schiessel, J. Rudnick, R. Bruinsma, and W. M. Gelbart, *Europhys. Lett.* **51**, 237 (2000).
- [119] F. Carlsson, P. Linse, and M. Malmsten, *J. Phys. Chem. B* **105**, 9040 (2001).
- [120] R. Messina, C. Holm, and K. Kremer, *Phys. Rev. E* **65**, 041805 (2002).
- [121] R. Messina, C. Holm, and K. Kremer, *J. Chem. Phys.* **117**, 2947 (2002).
- [122] R. R. Netz and D. Andelman, *Phys. Rep. Rev. Sect. Phys. Lett.* **380**, 1 (2003).
- [123] A. V. Dobrynin and M. Rubinstein, *Prog. Polym. Sci.* **30**, 1049 (2005).
- [124] R. Messina, *Phys. Rev. E* **70**, 051802 (2004).
- [125] R. Messina, *Phys. Rev. E* **74**, 049906(E) (2006).
- [126] R. Messina, *J. Chem. Phys.* **124**, 014705 (2006).
- [127] G. Decher, J. D. Hong, and J. Schmitt, *Thin Solid Films* **210/211**, 831 (1992).
- [128] G. Decher, *Science* **277**, 1232 (1997).
- [129] F. Caruso *et al.*, *Langmuir* **14**, 4559 (1998).
- [130] M. Onda, K. Ariga, and T. Kunitake, *Biosci. Bioeng.* **87**, 69 (1999).
- [131] A. Wu, D. Yoo, J. K. Lee, and M. F. Rubner, *J. Am. Chem. Soc.* **121**, 4883 (1999).
- [132] F. Caruso, R. A. Caruso, and H. Möhwald, *Science* **282**, 1111 (1998).
- [133] F. J. Solis and M. O. de la Cruz, *J. Chem. Phys.* **110**, 11517 (1999).
- [134] R. R. Netz and J. F. Joanny, *Macromolecules* **32**, 9013 (1999).
- [135] M. Castelnovo and J. F. Joanny, *Langmuir* **16**, 7524 (2000).
- [136] G. Ladam *et al.*, *Langmuir* **16**, 1249 (2000).
- [137] V. Panchagnula, J. Jeon, and A. V. Dobrynin, *Phys. Rev. Lett.* **93**, 037801 (2004).
- [138] V. Panchagnula, J. Jeon, J. F. Rusling, and A. V. Dobrynin, *Langmuir* **21**, 1118 (2005).
- [139] R. Messina, *Macromolecules* **37**, 621 (2004).
- [140] P. A. Patel, J. Jeon, P. T. Mather, and A. V. Dobrynin, *Langmuir* **22**, 9994 (2006).
- [141] R. Messina, *J. Chem. Phys.* **119**, 8133 (2003).
- [142] P. A. Patel, J. Jeon, P. T. Mather, and A. V. Dobrynin, *Langmuir* **21**, 6113 (2005).
- [143] J. L. Menchaca, B. Jachimska, F. Cuisinier, and E. Pérez, *Colloids Surf. A* **222**, 185 (2003).
- [144] J. J. Harris and M. L. Bruening, *Langmuir* **16**, 2006 (2000).
- [145] K. Binder, *J. Non-Equilib. Thermodyn.* **23**, 1 (1998).
- [146] H. Löwen, *J. Phys.: Condens. Matter* **13**, R415 (2001).
- [147] C. A. Murray, W. O. Sprenger, and R. A. Wenk, *Phys. Rev. B* **42**, 688 (1990).
- [148] S. Naser, C. Bechinger, P. Leiderer, and T. Palberg, *Phys. Rev. Lett.* **79**, 2348 (1997).
- [149] K. Zahn, J. M. Méndez-Alcaraz, and G. Maret, *Phys. Rev. Lett.* **79**, 175 (1997).
- [150] F. Ebert, P. Keim, and G. Maret, *Eur. Phys. J. E* **26**, 161 (2008).
- [151] A. Yethiraj and A. van Blaaderen, *Nature* **421**, 513 (2003).
- [152] L. Assoud, R. Messina, and H. Löwen, *Europhys. Lett.* **80**, 4801 (2007).
- [153] A. Blanco *et al.*, *Nature* **405**, 437 (2000).
- [154] J. Kecht *et al.*, *Langmuir* **20**, 5271 (2004).
- [155] F. Yan and W. A. Goedel, *Nano Lett.* **4**, 1193 (2004).
- [156] C. N. Likos and C. L. Henley, *Philos. Mag. B* **68**, 85 (1993).
- [157] T. Stirner and J. Sun, *Langmuir* **21**, 6636 (2005).
- [158] R. Messina and H. Löwen, *Phys. Rev. Lett.* **91**, 146101 (2003).
- [159] A. Barreira Fontecha *et al.*, *J. Phys.: Condens. Matter* **17**, S2779 (2005).
- [160] G. Goldoni and F. M. Peeters, *Phys. Rev. B* **53**, 4591 (1998).
- [161] B. Partoens, V. A. Schweigert, and F. M. Peeters, *Phys. Rev. Lett.* **79**, 3990 (1997).
- [162] I. V. Schweigert, V. A. Schweigert, and F. M. Peeters, *Phys. Rev. B* **60**, 14665 (1999).
- [163] I. V. Schweigert, V. A. Schweigert, and F. M. Peeters, *Phys. Rev. Lett.* **82**, 5293 (1999).
- [164] G. J. Kalman, P. Hartmann, Z. Donko, and K. I. Golden, *Phys. Rev. Lett.* **98**, 236801 (2007).

- [165] L. Świerkowski, D. Neilson, and J. Szymański, Phys. Rev. Lett. **67**, 240 (1991).
- [166] J. P. Eisenstein and A. H. MacDonald, Nature **432**, 691 (2004).
- [167] J. M. Pereira, P. Vasilopoulos, and F. M. Peeters, Nano Letters **7**, 946 (2007).
- [168] H. Totsuji, T. Kishimoto, and C. Totsuji, Phys. Rev. Lett. **78**, 3113 (1997).
- [169] M. Zuzic *et al.*, Phys. Rev. Lett. **85**, 4064 (2000).
- [170] B. V. Derjaguin and L. D. Landau, Acta Physicochim. (USSR) **14**, 633 (1941).
- [171] E. J. Verwey and J. T. G. Overbeek, *Theory of the stability of Lyophobic Colloids* (Elsevier, Amsterdam, 1948).
- [172] P. Pieranski, L. Strzelecki, and B. Pansu, Phys. Rev. Lett. **50**, 900 (1983).
- [173] M. Schmidt and H. Löwen, Phys. Rev. Lett. **76**, 4552 (1996).
- [174] M. Schmidt and H. Löwen, Phys. Rev. E **55**, 7228 (1997).
- [175] R. Messina and H. Löwen, Phys. Rev. E. **73**, 011405 (2006).
- [176] H. Löwen *et al.*, J. Phys.: Condens. Matter **17**, S3379 (2005).
- [177] L. Pauling, *The nature of the chemical bond* (Cornell, Univ. Press, New York, 1939).
- [178] F. Ramiro-Manzano, E. Bonet, I. Rodriguez, and F. Meseguer, Phys. Rev. E **76**, 050401 (2007).
- [179] A. B. Fontecha and T. P. H. Schope, Phys. Rev. E **76**, 050402 (2007).
- [180] A. Fortini and M. Dijkstra, J. Phys.: Condens. Matter **18**, L371 (2006).
- [181] J. Hong *et al.*, Adv. Mater. **19**, 4364 (2007).